UCRL-CR-120647

Attachment of Radon Progeny to Cigarette-Smoke Aerosols

A.H. Biermann
S.S. Sawyer

May 1995

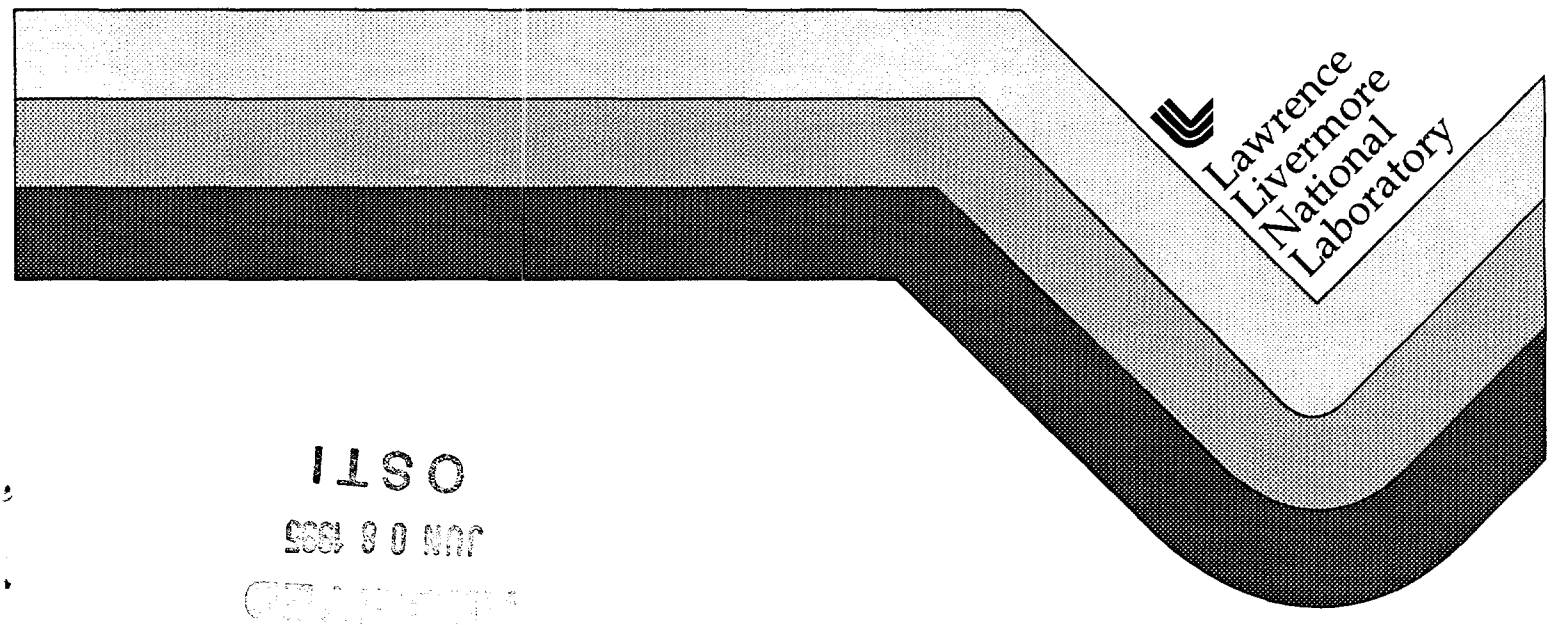

DISCLAIMER

Attachment of Radon Progeny to Cigarette-Smoke Aerosols

Arthur H. Biermann and Sterling R. Sawyer

Lawrence Livermore National Laboratory

May, 1995

ABSTRACT

The daughter products of radon gas are now recognized as a significant contributor to radiation exposure to the general public. It is also suspected that a synergistic effect exists with the combination cigarette smoking and radon exposure. We have conducted an experimental investigation to determine the physical nature of radon progeny interactions with cigarette smoke aerosols. The size distributions of the aerosols are characterized and attachment rates of radon progeny to cigarette-smoke aerosols are determined. Both the mainstream and sidestream portions of the smoke aerosol are investigated.

Unattached radon progeny are very mobile and, in the presence of aerosols, readily attach to the particle surfaces. In this study, an aerosol chamber is used to contain the radon gas, progeny and aerosol mixture while allowing the attachment process to occur. The rate of attachment is dependent on the size distribution, or diffusion coefficient, of the radon progeny as well as the aerosol size distribution. The size distribution of the radon daughter products is monitored using a graded-screen diffusion battery. The diffusion battery also enables separation of the unattached radon progeny from those attached to the aerosol particles. Analysis of the radon decay products is accomplished using alpha spectrometry. The aerosols of interest are size fractionated with the aid of a differential mobility analyzer and cascade impactor. Fractionation of the aerosol allows the dependence of aerosol particle size on attachment rate to be discerned.

The measured attachment rates of progeny to the cigarette smoke are compared to those found in similar experiments using an ambient aerosol. The lowest attachment coefficients observed, $\sim 10^{-6}$ cm^3/s, occurred for the ambient aerosol. The sidestream and mainstream smoke aerosols exhibited higher attachment rates in that order. The results compared favorably with theories describing the coagulation process of aerosols. Taking into account the size distributions of the aerosols, no significant differences in basic physical interactions between the radon progeny-smoke mixture and the progeny-ambient combination were found.

Introduction

It is estimated that there are 130,000 lung cancer deaths annually in the United States. Approximately 2,000 to 30,000 of these are attributed to exposure to radon gas. Epidemiology studies have attempted to assess the synergisms between cigarette smoking and radon gas exposure. However, the exact nature and degree of the synergism is not yet clear. It is one of the purposes of this study to elucidate any fundamental differences in physical interactions of radon progeny with a cigarette smoke aerosol as opposed to other aerosols.

Exposure to radon gas and its daughters is recognized as a health risk for the general population, especially those living in homes having elevated levels of radon gas. Epidemiological evidence of radon gas health effects comes from several studies involving miners(14-16). In U.S. uranium miners, the lung cancer rate was found to be 10 times higher than that of the general population (12,13); however, many of these cases involved smokers. Roscoe (16) found a 12-fold increase in the mortality ratio of nonsmoking uranium miners exposed to radon daughters when compared with nonsmoking nonminers.

Synergism between a physical agent and smoking is not to be unexpected. Selikoff (17) has shown an 8-fold increase in lung cancer risk due to asbestos workers who smoke as compared with nonsmoking asbestos workers. The multiplicative influence between radon exposure and smoking has been considered in the BEIR III(18) and ICRP(19) reports. Mathematical modeling of the lung cancer incidence in the U.S. miners seems to favor this relative risk, or multiplicative, approach (20,21). However, some follow-up studies(22-24) are suggesting the risk mechanisms are additive. Animal studies exploring the risks of cigarette smoke and ionizing radiation have proved largely inconclusive (25).

The behavior of radon and its daughter products in the environment is a complex and dynamic process. The radon daughter products are highly mobile and readily attach to any surfaces including those of aerosols in the surrounding gas. Many previous studies (10, 29, 30, 31, 33, 53, 54) on the attachment of radon daughters to aerosols involve the aerosol in the natural indoor environment. In these circumstances, many variables basic to the understanding of the physical attachment process are not controlled and perhaps not measured. These include the cleanliness of the surrounding gas with regard to vapors and trace gases, the size distribution of the radon daughters, the size and charge distribution of the aerosol, and the presence of other ions. In this study our experiments are performed in a laboratory environment where these parameters and others can be carefully monitored and controlled. Figure 1 illustrates the many interactions involved in a radon gas radon daughter, aerosol, gas/vapor, and surface system. The interaction represented by k_1 is the decay of radon gas to its daughter products. In the controlled laboratory environment certain interactions, such as daughter attachment to walls, k_{12}, and aerosol attachment to walls, k_{14}, can be studied separately. In this project, we are interested in the measurement for daughter/aerosol interactions, k_2 and k_3. The interactions of gas/vapor species with the daughter products, k_4 and k_5, are not measured, but their effects are monitored by

characterization of the size distribution of the unattached daughter products. In addition, special emphasis has been given to the measurement of the aerosol size distribution and the aerosol concentration, so that accurate daughter-to-smoke particle attachment rates can be measured.

Aerosols generated by cigarette smoke are likely to be larger in size than those found in the normal ambient air (26). The larger smoke particles having far greater surface areas would be expected to predominate in collecting unattached radon daughter activity. Furthermore, since the smoke particles constitute a liquid aerosol, the behavior of attachment and alpha recoil may differ from that expected for aerosols consisting of solid particles. It is suspected that the smoke aerosol would lead to altered deposition pattern and amounts of activity within the respiratory system.

It is the purpose of this research effort to investigate the attachment of radon daughters onto cigarette smoke aerosols. Both the sidestream and mainstream smoke aerosols are studied. Experiments are performed under controlled laboratory conditions. The experimentally measured attachment rates are compared with existing theories on particle attachment. The results are also compared to attachment rates on ambient aerosols to elucidate if there are any significant differences in the interaction of radon daughters with smoke versus a non-smoke indoor aerosol. The measurement of attachment and recoil rates of the radon daughters to/from the smoke aerosol can lead to improved quantitative predictions of radiation dose due to radon progeny.

Background

Indoor exposure to ^{222}Rn daughters can result in significant risk to the general public. The source of radon gas is radium in the earth. In a majority of cases, the principal pathway of radon into homes is through cracks and crevices within the building structure(31). Typical radon concentrations in U.S. homes are 0.2 to 4.0 pCi/L (28-30), although much higher levels have been observed in certain areas. The radiation dose received by individuals from radon gas is due to the deposition of daughter products in the respiratory system. The location and amount of deposition within the respiratory tract is complex physically because a portion of the daughter products can become attached to aerosol particles present in the environment. Radioactive decay of radon gas leads to the four daughter products, ^{218}Po (Radium-A), ^{214}Pb (Radium-B), ^{214}Bi (Radium-C), and ^{214}Po (Radium-C'). The two alpha emitters ^{218}Po and ^{214}Po are considered the major contributors to radiation dose in the respiratory system. The radioactive decay scheme for radon and its daughter products, part of the ^{238}U series, is presented in Figure 2.

Radon gas decays to ^{218}Po releasing a 5.48 MeV alpha with a half-life of 3.8 days. The ^{218}Po is formed as a recoiling atom having an energy of 90 keV with a recoil range of 50 to 100 μm in air(3). After recoil, the ^{218}Po ion has been observed to be both positively- and negatively-charged (4,5,56). As an ion, ^{218}Po is very mobile an active. Its diffusion coefficient has been measured by many workers with values from .03 to .06 cm^2/s (5-7).

An uncharged ^{218}Po molecule of 3.8 Angstroms in diameter would be expected to have a diffusion coefficient of 0.14 cm^2/s. Thus, the lower, measured diffusion coefficients indicate that ^{218}Po has formed clusters with other available gas species in the environment. Such species might include water vapor, carbon dioxide, oxygen and trace gases (8,9). Since the clustering and size of the final ^{218}Po may vary greatly in differing environments, it is no surprise that a range of mobilities has been observed. Because of their high mobilities, both individual and clustered ^{218}Po atoms readily attach to any aerosol particle in the environment. The rate of attachment depends on the diffusion coefficient of the unattached ^{218}Po atom or cluster, and the number and size of the aerosol particles.

^{218}Po has a half-life of 3.1 min and decays to ^{214}Pb by a 6.00 MeV alpha with a recoil energy of about 110 keV. Several possibilities for the ^{214}Pb exist depending on the location of its ^{218}Po precursor. If the ^{218}Po was previously attached to an aerosol particle, it may recoil from the particle back into the air; it may penetrate into the particle; it may penetrate through the particle if the particle is very small; or it may diffuse into the particle if the particle is a liquid like cigarette smoke. In modeling efforts, most investigators assume that the recoil factor, the fraction of decays in which the daughter escapes back to the surrounding gas, is between 0.5 and 1 (10,11,47,48). However, in the case of liquid particles, the recoil factor may be less than this(46).

The daughter ^{214}Pb, which has a half-life of 26.8 min, further decays to ^{214}Bi by beta and gamma emission. ^{214}Bi is also a beta and gamma emitter. It has a half-life of 19.7 min, and decays to ^{214}Po. ^{214}Po is the final decay product in the chain having a half-life of only 1.6×10^{-4} s. It decays to Pb-210 by a 7.68 MeV alpha.

The half-lives of the radon daughter products are comparable in magnitude to aerosol interactions such as particle coagulation and attachment, particle surface deposition, and air-cleaning processes. The radioactive decay and attachment processes occur simultaneously and lead to increased complexity when attempting to model the process and predict radiation dosage. In many uncontrolled indoor environments, the equilibrium of the radon daughter activities may never be reached because of changes in aerosol size and concentration. A theoretical model describing this dynamic behavior of the radon/radon daughter and aerosol system was first developed by Jacobi (32) for applications to uranium mines. It was later modified by Porstendorfer (33) for application to indoor housing-type environments. The theoretical model includes the radioactive decay scheme described above, daughter attachment to an aerosol, room ventilation, and radon daughter deposition to surfaces, and aerosol deposition to surfaces. This model is readily adaptable to our laboratory chamber experiments. Following Porstendorfer, the rate equations for the free and attached radon daughter products can be written as

$$\frac{dC_j^f}{dt} = \lambda_{j-1} C_{j-1}^f + p_{j-1}\lambda_{j-1} C_{j-1}^a - (\lambda_v + \lambda_j + \lambda_a + \lambda_w^f) C_j^f \qquad \text{(Eq. 1)}$$

$$\frac{dC_j^a}{dt} = (1-p_{j-1})\lambda_{j-1}C_{j-1}^a + \lambda_a C_j^f - (\lambda_v + \lambda_j + \lambda_w^a)C_j^a$$

(Eq. 2)

where

C_j^f = the concentration of the jth free (unattached)radon daughter product ($C_0^f = C_0$ denotes the concentration of radon gas),

C_j^a = the concentration of the jth free (unattached)radon daughter product ($C_0^a = 0$),

λ_V = ventilation rate,

λ_j = radioactive decay rate of the jth radon daughter, (λ_0 is the decay rate for radon gas),

λ_w^f = rate of the free daughter plate-out to the walls,

λ_w^a = rate of the attached daughter to the walls (or plate-out),

λ_a = attachment rate of the daughter products to the aerosol, and

p_j = probability of detachment (or recoil parameter) for the jth daughter product.

The first equation describes the rate of change in concentration of the free daughter products, while the second describes that for the attached radon daughters. Loss mechanisms for a free daughter include the processes of ventilation, decay to the suceeding daughter, attachment to aerosol particles, and attachment to other fixed surfaces. Radon daughter attachment to the aerosol is assumed to be the same for all daughters. For purposes of modeling our experimental apparatus, we have assumed that gas venting from the environment is clean and free from radon. The parameters in this model are λ_a, p_j, λ_w^f, and λ_w^a. These parameters are not measured directly, but must be calculated from the measured concentrations of other species. The probability, p_i, allows for the detachment of an attached radon daughter from an aerosol particle during the decay process. The detachment probability is only a concern for the alpha emitter daughters; thus $p_0 = p_2 = p_3 = 0$. Equilibrium is assumed to be the case in most field and laboratory studies so that the parameters can be solved analytically. We will demonstrate this to be the case for these experimental studies.

Applying Equations 1 and 2 to the ^{218}Po daughter, we can write for the change in concentration of the free and attached atoms:

$$\frac{dC_1^f}{dt} = \lambda_0 C_0 - (\lambda_v + \lambda_1 + \lambda_a + \lambda_w^f)C_1^f$$

(Eq. 3)

$$\frac{dC_1^a}{dt} = \lambda_a C_1^f - (\lambda_v + \lambda_1 + \lambda_w^a) C_1^a \ .$$

(Eq. 4).

Once steady-state is achieved, the equations can be simplified:

$$\lambda_v + \lambda_1 + \lambda_a + \lambda_w^f = \frac{\lambda_0 C_0}{C_1^f}$$

(Eq. 5)

$$\lambda_a = (\lambda_1 + \lambda_v + \lambda_w^a) \frac{C_1^a}{C_1^f} \ .$$

(Eq. 6)

The latter, Equation 6, results in the best method for calculating the aerosol attachment rate. Both the free and attached daughter activity concentrations ($=\lambda_j C_j$) in the air are measured quite accurately in our studies. The rate of deposition of the attached progeny to the chamber walls, λ_w^a, can be determined by measurement of the aerosol decay in a static environment. The ventilation rate can be determined by measuring the air concentration of radon gas, or the daughter products once equilibrium has been established. The deposition rate of the free daughters to the wall is not required. However, after the aerosol attachment rate is determined, the free daughter deposition rate can be found by Equation 5.

In the case of heterodisperse aerosols such as the cigarette smoke aerosols, the attachment rate in the model for describing the radon progeny dynamics is really an "effective" attachment representing all particle sizes given by

$$\lambda_a = \int_0^\infty N(d) \beta(D_f, d) \delta d$$

(Eq. 7)

where

$N(d)$ = the size distribution of the aerosol ($\int_0^\infty N(d)\delta d = 1$),

$\beta(D_f, d)$ = the attachment rate,

d = diameter of the aerosol particle, and

D_f = diffusion coefficient of the free radon progeny.

The attachment phenomenon of radon progeny to aerosols can be considered a coagulation process, where the progeny are considered to be very, very small particles. Coagulation is caused by mechanisms, such as Brownian motion, turbulence, and external fields, which

bring about a relative velocity between aerosol particles. In our case, Brownian motion is the major mechanism leading to significant relative velocity between the small progeny and the much larger aerosol. As part of this study, we have compared measured attachment rates to three theoretical models describing the attachment process as derived according to the coagulation theory of aerosol physics. These models are the kinetic, Smoluchowski, and Lassen and Rau. Our experimental data has been compared to these theoretical models which predict attachment coefficients. The first model is based strictly on kinetic theory and according to (41) can be expressed as

$$\beta(D_f, d) = \frac{\pi d^2}{4} v\alpha = \frac{\pi d^2}{4}\left[\frac{8kT(M_f + M_a)}{\pi M_f M_a}\right]^{0.5}\alpha \qquad \text{(Eq. 8)}$$

where

$\beta(D_f, d)$ = the attachment coefficient (cm^3/s),
v = mean kinetic speed,
d = diameter of an aerosol particle,
α = progeny-to-particle sticking probability,
M_f = mass of the free progeny,
M_a = $\rho\pi d^3/6$ = mass of the aerosol particle,
ρ = aerosol particle density,
T = temperature, and
k = Boltzman's constant.

In this model the attachment rate of the radon progeny is directly proportional to the available surface area of the aerosol. The model is valid in the non-continuum (or free molecule) region where the Knudsen number (ratio of the mean free path of the gas to the aerosol radius) approaches infinity (>10). Thus, this model is applicable for particles having sizes less than 10 nm in diameter.

The second model, first developed by Smoluchowski and taken from Hidy(51), is the classical coagulation theory for aerosols by Brownian motion. It can be expressed as

$$\beta(D_f, d) = 2\pi(D_a + D_f)(d + d_f) \qquad \text{(Eq. 9)}$$

where

D_a = the diffusion coefficient of the aerosol particles, and
d_f = the diameter of the free radon progeny.

The diffusion coefficient is given by

$$D = \frac{kTC_s}{3\pi\eta d} = \frac{kT}{3\pi\eta d}\left[1+\left(\frac{\ell_g}{d}\right)\left(2.514+0.8\exp^{\frac{-0.55d}{\ell_g}}\right)\right]$$

(Eq. 10)

η = viscosity of the gas,

C_s = Cunningham slip correction for the aerosol particle, and

ℓ_g = the mean free path of the gas.

The diffusion coefficient for an aerosol with diameter 0.1 μm is 3.5×10^{-6} cm^2/s, far less than an unattached radon progeny whose the coefficient is typically 0.05 cm^2/s. This classical coagulation model is valid in the continuum range where Knudsen number $\rightarrow 0$ (<0.1), that is for particle sizes greater than 1 μm in diameter. Variations on the classical model, but not considered here, include the effects of particle charge and air turbulence.

The third model considered, developed by Lassen and Rau(42), lends itself to be applied in the submicron aerosol region. Following Junge(49), the attachment rate can be expressed as

$$\beta(D_f,d) = \left(\frac{\pi d^2}{4}\right)\frac{v}{\left(1+\frac{vd^2}{8D_f(d+2\ell)}\right)}$$

(Eq. 11)

where

D_f = diffusion coefficient of the free progeny and

ℓ = the mean free path of the free progeny.

This expression is similar in form to the kinetic expression, but contains a correction term in the denominator which depends on the particle diameter and the diffusion coefficient of the radon progeny. Attachment rates predicted by this model approach those of the kinetic model for attachment to small aerosol particles (<0.1 μm in diameter) but are less than those of the kinetic model for larger aerosols (>1.0 μm).

A comparison of the three coagulation models are presented in Figure 3. The coagulation coefficients calculated are for free daughters having diameter 1 nm colliding with various aerosol particle sizes (the independent variable in the figure). Associated parameters used to evaluate the models include α=1, T=293°K, $M_f=5.2\times10^{-24}$ cm^3, D_f=0.05 cm^2/s, $\ell=1\times10^{-6}$cm, $\ell_g=6.53\times10^{-6}$ cm, and $\eta=1.83\times10^{-4}$ g/cm-s. The diffusion coefficient and mass correspond to a clustered formation containing one free polonium progeny and 6 water molecules. The coagulation coefficient increases markedly for larger aerosol particles. The Lassen and Rau model serves to bridge the gap between the kinetic and the classical aerosol

coagulation theories in the submicron range, the size of the cigarette smoke aerosols in this study. In a typical environmental setting having an aerosol with diameter 0.1 μm, the coagulation coefficient is about 1×10^{-6} cm^3/s. If there are 10^4 particles/cm^3 present, the resulting attachment rate is 0.01/s.

Experimental

Our radon progeny-cigarette smoke attachment experiments are performed in a 2,000 l stainless steel aerosol chamber. A general block diagram of the experimental apparatus is shown in Figure 4a. A more detailed diagram is provided in Figure 4b. Radon gas is obtained by emanation from a 10 mCi ^{226}Ra powder source. The radium source is contained in a U-tube and confined by both 25-mm diameter glass fiber and sintered metal filters. An automatic valving system on the inlet and outlet of the U-tube allows the radium source to be purged with gas and guarantees safe and correct operation. Proper shielding of the radium source is provided to prevent worker exposure to radiation. The radon generation system and the aerosol chamber are housed in a confinement area that is cordoned off from the work area by a plastic curtain. The confinement area is served by an auxiliary ventilation system designed to keep the pressure of the confinement area negative with respect to other rooms in the building. Charcoal traps and high efficiency particulate air filters are used to control the release of radon and airborne daughter products to the atmosphere. Two continuous air monitors monitor, real-time monitors for alpha activity, sample the exhaust from the confinement area and alarm in the presence of significant levels of activity.

The resulting purge gas from the radium source, now containing radon, is collected on carbon traps with a portion delivered to aerosol chamber. Prior to radon gas entry, the chamber is pre-conditioned with clean air including an aerosol if desired. In pre-conditioning the chamber gases are passed through a carbon trap, a molecular sieve, and a high efficiency air filter. Tests have shown that particle concentrations less than 0.05/cm^3 can be attained within the chamber. Once purged with air, filtered radon is introduced into the chamber. For these experiments radon levels ranging from 100 to 3000 pCi/l (3.7 - 110 Bq/l) were used. The chamber is maintained at a slight positive pressure to prevent any leakage of the ambient air into the chamber; this guarantees that the measurements made are performed on the aerosol present in the chamber. Two fans are available in the chamber to provide for brief mixing at the beginning of an experiment or for continued mixing to induce artificial turbulence in the chamber. In general air sampling of the chamber environment does not begin until equilibrium of the daughter products is reached. Total radon daughter activity concentrations are measured by withdrawing air samples of chamber gas through membrane filters. Typically, 25-mm diameter Millipore mixed-cellulose-ester filters having a 0.45 μm pore size are used. Periodic sampling verifies equilibrium conditions have been reached in the aerosol chamber. Filter samples are analyzed by alpha spectrometry in the alpha-gamma radiation detection system described below.

A range of size distributions for cigarette smoke aerosol has been reported in the

literature(26). Mainstream smoke has been reported to have mass median aerodynamic diameters of 0.25 to 0.7 μm with geometric standard deviations from 1.2 to 1.64. The aerosol from sidestream smoke may be somewhat smaller(59). Significant portions of smoke aerosols have been found to be greater than 1 μm in diameter(42). In our experiments, the cigarette smoke aerosol is generated using a single cigarette machine fabricated by the University of Kentucky Tobacco and Health Research Institute(60). The smoke generator can deliver either the sidestream or mainstream into the aerosol chamber. The mainstream smoke is that portion which is drawn through the cigarette and inhaled by the smoker; the sidestream is that from a burning cigarette that is released to the environment between puffs. It has been estimated that the sidestream fraction accounts for 95% of the cigarette smoke found in the ambient surrounding (2). University of Kentucky 2R1 reference cigarettes are used for generation. The cigarette smoke generator is operated at 1 puff per min. Each puff is 35 ml in volume and 2.1 s in duration resulting in a flow rate of 1 lpm. The sidestream flow rate is 1.8 lpm.

In our experiments, we use a number of instruments to characterize the smoke aerosol. The size distribution of the smoke aerosol is monitored with a Thermo Systems, Inc., Model 3071 differential mobility analyzer and/or a Particle Measurement Systems Model ASASP-X laser spectrometer. The mobility analyzer can measure particle size in the range from 0.01 to 0.5 μm in diameter and the laser spectrometer in the range from 0.1 to 3.0 μm diameter. We use another instrument, a Thermo Systems, Inc., Model 3020 condensation nucleus counter, to measure the number concentration of aerosol particles. The counting efficiency of the nucleus counter decreases dramatically for particles less than 10 nm in diameter. It easily demonstrated that the nucleus counter does not detect the progeny by sampling the chamber air with only free progeny present. In the presence of an aerosol, the effect can be verified by placing several diffusion battery screens in the sample line prior to the counter and verifying that the particle concentration does not decrease. Thus, only the aerosol particles and not the unattached radon progeny are counted with this instrument.

Free radon progeny, that which has not attached to aerosol particles, exist in clusters having sizes in the nanometer diameter range. To measure their size distribution, or diffusion coefficient spectrum, we have fabricated a graded-screen diffusion battery. The use of graded-screen diffusion batteries for the measurement of the distribution in diffusion coefficient of the radon progeny has been described by other investigators (34,35,40). The battery used here is a 6-stage device consisting 16, 50, 80, 200, 325, and 500 mesh stainless-steel screens 25 mm in diameter. The 6 stages are stacked in a series arrangement and are operated at a volumetric flow rate of 4 lpm. Air samples are taken with the diffusion battery installed in a port in the chamber wall to prevent deposition that would occur if any sampling transport lines were used. Size fractionation occurs by the smaller mesh screens collecting those progeny having the greatest diffusion coefficients. A 25-mm diameter backup membrane filter is placed in series after the battery to collect activity penetrating the screens. The battery is not a differential-type collection device, so the activity data on the screens must be deconvoluted to attain size distributions. We use a modified version of the expectation maximization algorithm (37) to perform the

deconvolution or inversion process. Input to the algorithm includes the activity measured on the screens and the penetration function of each collection screen. The expected penetration through each screen is calculated according to Cheng (36) with knowledge of certain physical characteristics of the screens. The parameters required to calculate the penetrations for our diffusion battery and the penetration functions are provided in Appendix A. A size array from 0.2 to 40 nm having equal logarithmic intervals is used in the inversion process. Because of the nature of the diffusion collection process, some daughter products are also collected on the back of the screens. As part of our data collection, both the fronts and backs of the screens are counted to account for the total activity. With this measurement technique, the diffusion coefficient spectrum of the radon daughters is attained over the range 0.0001 to 0.5 cm^2/s. In previous studies involving no aerosols, we have demonstrated that the diffusion battery is very efficient at the collection of the free progeny; only 0.4%, 0.5%, and 1.3% of the total activities for the unattached ^{218}Po, ^{214}Pb, and ^{214}Bi penetrate the diffusion battery and collect on the backup filter. Activity that has attached to much larger aerosol particles easily penetrates through the screens and is also collected on the filter. Therefore, the battery is an excellent separator for activity that is free (or in the form of clusters) from activity that is attached to aerosols. Progeny concentrations determined from diffusion battery air samples allow us to calculate attachment rates experimentally.

To determine activity-size distributions of the radon progeny that have attached to the cigarette smoke aerosols, a Model 100 micro-orifice rotating cascade impactor (MSP Corporation) is used. The particle collection stages of conventional impactors accumulate particle deposits in discrete areas immediately under the impaction jets. The collection stages of the rotating impactor move to attain uniform particle deposition across the collection surface, a requirement for the subsequent analysis of alpha activity. We operate the impactor with 8 stages and a 37-mm diameter backup filter to capture particles which have penetrated the stages. At the sample rate of 20 lpm used in these experiments the 50% cut-points for the stages are 9.9, 2.2, 1.24, 0.66, 0.38, 0.23, 0.14, and 0.10 μm aerodynamic diameter. Because of their high mobility there is a possibility that some free progeny might be collected on the collection stage of the impactor. Tests were conducted collecting free progeny in the absence of aerosol to investigate the magnitude of this effect. Only about 0.25% of free progeny is collected on the 7 impactor stages used in these experiments.

To measure the activities of collected radon daughter products, we have developed an alpha/gamma radiation detection system (38). Because the half life of the ^{218}Po daughter is very short, the radon progeny activities must be measured immediately after their collection. The detector system illustrated in Figure 5 consists of 8 detector units to facilitate the analysis of several samples in parallel. For example, all the screens from a diffusion battery air sample and filter can be processed simultaneously. Each detector unit consists of a semiconductor surface-barrier diode to detect alpha decays and a NaI(Tl) scintillator to detect gamma rays. The pulse height data from all of these detectors are multiplexed and record in a single multichannel buffer that is interfaced to a personal computer. The amounts of ^{218}Po and ^{214}Po are determined from the 6.00- and 7.68-MeV alpha particles,

respectively. The detection efficiency of the alpha detectors is approximately 30%. The gamma activities of the ^{214}Pb and ^{214}Bi decays are usually near background in these studies, however their activities can be determined from other alpha activities. The ^{214}Bi activity can be inferred directly from the ^{214}Po activity since the ^{214}Po half-life is very short. The ^{214}Pb activity is determined from the ^{218}Po and ^{214}Po measured activities. Its activity is obtained by taking 2 accumulations at different times and solving the relevant decay equations. Several computer programs written in QuickBasic are available to effect the operation of the detector system(39): These include 1) a calibration program to facilitate the energy calibration and determine detector efficiencies, 2) a program used to control data acquisition and storage, and 3) a program for data reduction. The latter calculates the air concentration of the progeny correcting for the decay of the progeny during sampling, after sampling, and during the counting period. Our filter sampling of the radon progeny and spectrometry detection and analysis system has been verified in a workshop hosted by the Environmental Measurements Laboratory(EML) in 1989 (27). Potential alpha energy concentration levels were found to be within 6% of EML values. Radon gas is measured with an ion chamber.

We have discussed how the graded-screen diffusion battery can be used to separate the unattached radon progeny from those that have attached to the aerosol. However, to further characterize the attachment phenomenon to the specific aerosol, it is necessary to size fractionate the aerosol and measure the activity in the size fractions. Two experimental methods for achieving the aerosol size separation, both using the differential mobility analyzer, were used in these studies. The methods are illustrated in Figure 6. The particular method used depends on the size range of interest of the smoke aerosol. In the first method, the mobility analyzer can be used in the aerosol production stage. Here, the smoke aerosol is passed through the analyzer prior to entering the chamber. Since the chamber would then have a very narrow size distribution of particles, no size separation of the aerosol is required during subsequent sampling. In the second technique, the smoke aerosol is generated and passed directly into the chamber leading to a heterodisperse aerosol to be sampled. Fractionation of aerosol is then accomplished by the mobility analyzer during sampling of the chamber environment. In both methods the particle concentration corresponding to the measured activity on the particles can be obtained with the condensation nucleus counter. The rotating impactor can also be used for size separation, but it is not amenable to having particle concentrations measured between collection stages.

In the experiments we have characterized the radon daughter attachment to both sidestream and mainstream smoke aerosols. We have compared these measurements to those involving the attachment to the laboratory ambient aerosol. Final attachment rates/coefficients are determined by calculation using the equilibrium model for radon progeny, Equation 6.

Results

In any investigation of the attachment of radon progeny to aerosols, it is important to begin with the characterization of the aerosol size distribution. For most of our experiments involving the cigarette smoke aerosols, the laser spectrometer is used alone. However, because some of the cigarette smoke is less than the minimum detectable size of the spectrometer (about 0.1 μm diameter), we performed a more detailed size characterization using the spectrometer in combination with the differential mobility analyzer. Examples of the size distributions for the sidestream and mainstream smoke aerosols is shown in Figure 7. The geometric count median diameter for the sidestream and mainstream distributions is 0.15 μm and 0.30 μm respectively. For both aerosols, the geometric standard deviation lies between 1.8 and 1.9. Typically, standard deviations of the smoke aerosols are less when measured with only the laser spectrometer since particles in the lower tail of the distribution are not detected. Under these circumstances, the mainstream smoke may exhibit a broader distribution, since a larger fraction of its distribution is detected.

Of equal importance is the characterization of the unattached radon progeny. Our chamber is a clean environment so that the diffusion coefficient spectra of the progeny can be controlled. Typical radon progeny produced in this test chamber have a very narrow and reproducible size distribution centered at approximately 1 nm in diameter. Examples of the radon daughter size distributions for the ^{218}Po, ^{214}Pb, and ^{214}Bi progeny are presented in Figure 8. The distributions were obtained using activity data from graded-screen diffusion battery and sampled from an environment of clean, filtered air, that is, without any aerosol present. The ^{218}Po activity is distributed very sharply at a diameter near 1 nm, corresponding to a diffusion coefficient of 0.045 cm^2/s. The location of this peak for ^{218}Po is similar to that found in field measurements and thus serves as a realistic progeny to use in laboratory studies. The diffusion coefficient is less than what would be expected for a free atom; it is likely attached to a water cluster of 4-6 molecules. Standard deviations indicate a near monodisperse size distribution. In comparative studies (50), typical ^{218}Po diffusion spectra in the chamber were found to have sharply defined spectra with geometric standard deviations ranging from 1.001-1.1.

In the presence of an aerosol the radon progeny rapidly attach to the aerosol. Inversion of the graded-screen battery data with aerosol present results indicates a bimodal activity distribution. Figure 9 illustrates and example. In this example, the activity associated with the free daughters (< 1 nm) is the minor mode. Most of the activity is present on the aerosol which is depicted in the maximum size interval of the diffusion battery size array. About 92% of the activity has attached to the aerosol. However, the battery is not capable of resolving the activity attached to the aerosol because the aerosol distribution is greater than the useful range of the battery.

The activity attached to the aerosol is readily resolved by sampling with the rotating cascade impactor. Examples of the ^{218}Po activity-size spectrum sampled with the rotating impactor are illustrated in Figure 10. Here, the progeny attachment to the sidestream and

mainstream cigarette aerosol and laboratory ambient aerosol are contrasted. All distributions are distinctly bimodal illustrating clearly the free radon progeny at approximately 1 nm in diameter and the attached fraction on the aerosol particles occurring in the 0.05 - 2.0 μm diameter range. The free progeny mode remains extremely sharp as in the case of no aerosol. Now that aerosol is present the majority of the activity has move from the free mode to the aerosol mode. The activity geometric median diameters are 0.22 and 0.29 μm for the sidestream and mainstream smoke aerosols, respectively. Corresponding geometric standard deviations are 1.6 and 2.0 for the sidestream and mainstream, respectively. Thus, the activity attached to the mainstream smoke occurs at slightly larger particle sizes and the distribution is considerably broader. In a recent study on radon attachment to cigarette smoke (52), median diameters of 1.19 nm for the free progeny and 0.1 μm for the aerosol were measured. In contrast to the smoke aerosols, the activity-size distribution for the ambient aerosol has an activity median diameter of 0.12 μm diameter and a standard deviation of 1.9. The ^{214}Pb and ^{214}Bi progeny (not shown) have similar distributions with the exception that, in the smoke case, they have even more activity associated with the smoke particles.

After radon gas and the aerosol have been introduced into the chamber, periodic sampling can be performed to ensure that an equilibrium condition has been attained. Two illustrations of periodic sampling over a period of 5-6 hours are presented in Figure 11. The first illustration (a) indicates the activity concentration for the three progeny ^{218}Po, ^{214}Pb, and ^{214}Bi with no aerosol present. Data markers represent calculated activities based on air samples taken at the indicated times. The theoretical model, Eq. 1, is depicted by the solid lines. Radon gas was introduced into the chamber at time zero, after which the progeny form rapidly reaching equilibrium conditions within 1 hour. All progeny indicate a slight continual decrease in concentration for the remaining of the evaluation period. This results from allowing clean air to enter the chamber to replace the sampled air. In this case, the ventilation rate, λ_V, is 0.0013/min. The second illustration (b) shows the unattached progeny fraction in an experiment with aerosol present. The ^{218}Po and ^{214}Pb daughters have still achieved equilibrium within 1 hour. In our experiments we wait approximately 2 hours before making attachment rate measurements.

In the presence of no radon, we attempted to measure the aerosol deposition rate, λ_w^a. In experiments using the mainstream smoke aerosol, we determined the deposition rate to be less than 0.001/min. Particle concentrations were determined with the condensation nucleus counter. The actual sampling prevented a value less than this to be measured. Nevertheless, this rate is far less than the ^{218}Po decay rate of 0.227/min; thus, for these experiments, the loss of aerosol to the walls is inconsequential in the determination of the progeny attachment rate to the aerosol. In a similar experiment with the two chamber fans, the aerosol deposition was determined to be approximately 0.0005/min. The measured deposition rates also include any decrease in particle concentration due to coagulation of the aerosol with itself. Thus, coagulation is not a significant factor in these measurements. Values of the aerosol deposition rate would be expected to be similar for the sidestream cigarette smoke since its distribution is not that dissimilar from that of the mainstream.

The deposition rate of free progeny to the chamber walls can be determined in experiments involving no aerosols. The deposition rate, λ_w^f, was determined using Eq. 5, with $\lambda_v=\lambda_a=0$. In the static chamber environment we measured free progeny deposition rates of 0.1-0.3/min. The deposition velocity of the free progeny to the surface, w^f, can be calculated using $w^f=\lambda_w^f/S_r$ where S_r is the surface-to-volume ratio of the chamber. Using $S_r=0.005$, we arrive at deposition velocities from 0.3-1 cm/s. Such values are in the range of measurements by other investigators (44,55). In the presence of induced turbulence by the fans, the higher rates of 0.6 to 1.5/min were observed.

However, the induced turbulence did not result in a significant increase in the attachment rate of the progeny to aerosol particles. A theory proposed by Saffman and Turner (57) predicts increased coagulation due to differential velocities between particles caused by inhomogeneities from the eddy fluid motion and by differing inertia caused by unequal particle size. In more recent work(58), small particles coagulating onto much larger ones in the presence of turbulence is also considered. Although there is a great size differential between the radon progeny and the smoke aerosol, there is not necessarily an increase in the relative velocities between the free progeny and those attached to aerosols. If both the free progeny and the aerosol follow the inhomogeneities due to the turbulence, then increased coagulation or attachment would not be expected. Since the smoke aerosols studies lie in the submicron size range, this is the case here.

To elucidate the dependence of attachment rate on particle size, the heterodisperse smoke aerosol was generated and allowed to equilibrate with the radon progeny. The differential mobility analyzer was used to sample from the chamber and fractionate the aerosol into discrete size intervals. The fractionated aerosol was collected on a membrane filter to determine the activity concentration and the particle concentration of the fractionated aerosol was measured with the condensation nucleus counter. Because of the size selectivity of the mobility analyzer, the number of particles in a given interval are far less than that occurring in the chamber. From the measurements the activity per particle can be calculated. Figure 12 compares the results of the smoke size fractions with similar experiments on the laboratory ambient aerosol. Much of the scatter in the data (indicated by data markers) results from the low particle counts in the aerosol fractions. If it is assumed that the attachment process depends on a simple power function of particle size (attachment $\propto d^n$), then the slope of a relationship in this graph is indicative of that power. Pure surface attachment ($n=2$) as predicted by the kinetic theory (Equation 8) is indicated by a dotted line. Regression analysis of the smoke data results in a slope of 1.5, somewhat less than expected for pure surface attachment.

The above technique of studying the attachment-size relationship does not readily lend itself to the determination of absolute attachment rates or attachment coefficients. However, we have determined absolute attachment rates of the progeny to the aerosols using heterodisperse aerosols and in one case, a 0.1-μm-diameter fraction of the smoke aerosol.

The latter was generated by filtering the smoke aerosol through the differential mobility analyzer. Results of our measurements and comparison with the theoretical expressions for aerosol coagulation are presented in Figure 13. Depending upon the aerosol, attachment coefficients range from 8×10^{-7} to about 5×10^{-6} cm^3/s. Ranges in the attachment coefficient are indicated by the vertical and horizontal lines through data points. Ranges shown for the size were chosen using estimates of the count and activity median diameters for the aerosols. Ranges given for the attachment coefficient values is that encompassing a number of experimental measurements. The mainstream smoke aerosol exhibits attachment coefficients somewhat greater than the sidestream because of its slightly greater size distribution. And, attachment coefficients for the sidestream smoke are greater than those for the ambient aerosol. This can also be attributed to size since the sidestream particle distribution is somewhat larger than the ambient aerosol studied. On the other hand, the coefficient determined for the 0.1-μm-diameter fraction is approximately 1×10^{-6} cm^3/s, essentially the same as the value for the laboratory room aerosol.

Experiments carried out using lower concentrations of radon gas, 100-300 pCi/l did demonstrate any changes in the attachment coefficients. None would be expected by the theory described above; such a result is corroborated by measurements of George(43,44) and Subba Ramu(45).

We can quantify the effect that the standard deviation of the aerosol causes on the overall attachment coefficient by using Equation 7. Assuming a lognormal size distribution function to represent the aerosol distribution, we have graphed Figure 14(a) the theoretical attachment coefficient according the Lassen and Rau expression (Equation 11) as a function for the aerosol number median diameter, n_m. The family of curves represents different values for the geometric standard deviation, σ_g, of the distribution. Values of parameters used in the model are those used for the calculations presented in Figure 3. The curve having a σ_g=1.1 yields a coefficient only 1% greater than that for a monodisperse aerosol (σ_g=1.0). Calculated coefficients for the wider distributions, σ_g=2.0 and σ_g=3.0, are about 1.4 and 2.0 times the monodisperse case respectively. Environmental tobacco smoke is a combination of the ambient (non-smoke) and cigarette smoke aerosols, and the aerosols are in competition for attachment of radon progeny. Figure 14(b) illustrates this effect of by combining lognormal distributions of a smoke and ambient aerosol and increasing the proportion of the smoke (number) concentration. A hypothetical ambient aerosol is chosen having a lognormal distribution with parameters n_m=0.1 μm diameter and σ_g=2.0. The smoke aerosol geometric standard deviation was taken as 2.0. The result, again integrating Equation 7, indicates that a smoke aerosol having a number median diameter of 0.2 μm (like those encountered in this study), can exhibit attachment rates 3 (50% of the aerosol is smoke) to 4.5 (90% of the aerosol is smoke) times greater than ambient aerosol alone. For a larger smoke aerosol, , greater increases are indicated with increased rates of 5 and 9 over the ambient aerosol for 50% smoke and 90% cases respectively.

Conclusions

The attachment rates of the radon progeny to mainstream and sidestream cigarette smoke aerosols have been measured. Attachment coefficients have been compared to those for a laboratory room aerosol and to theoretical expressions for aerosol coagulation. Measurements, conducted in chamber where the aerosols and progeny and their environment could be controlled, were made after equilibrium conditions had been attained.

Activity distributions indicate distinct bimodal size distributions with modes corresponding to the free radon progeny and progeny that has attached itself to the cigarette smoke particles. Activity of the free progeny occurs at about 1 nm in diameter and is near monodisperse. Activity of the attached progeny, occurring in the submicron size range between 0.1-0.4 μm in diameter, corresponds to the distribution of the smoke particles and is heterodisperse. The radon daughter activity attached to the mainstream cigarette smoke aerosol was found to be attached to somewhat larger particles.

The attachment rate of the progeny to the smoke aerosol in a static environment was compared to one with induced turbulence. Although the deposition rate of the free progeny to the chamber walls increased substantially, no significant increases in attachment rate of the progeny to the aerosol particles were found.

Measured attachment coefficients for the smoke and laboratory ambient aerosol have values of approximately 10^{-6} cm/s in magnitude and compare favorably to coagulation coefficients calculated by theory. The mainstream smoke exhibited the highest measured attachment coefficients followed by the sidestream and the room aerosol. Attachment coefficients for the mainstream smoke were up to 4 times greater than those for the ambient aerosol alone. The measured attachment coefficients compare favorably with the Lassen and Rau theoretical expression for progeny attachment to submicron aerosols, where the attachment rate is proportional to somewhat less than an expected pure surface area, or kinetic, theoretical relationship. Differences in the attachment coefficients for the sidestream and mainstream cigarette aerosols and the room aerosol were demonstrated to be the result of the differing particle size distributions of the aerosols. The attachment rate further depend on the concentration of smoke particles, since the smoke aerosol is in competition with the aerosol of the environment.

In real situations, the size distribution of the smoke aerosols is likely to be dependent on the type of cigarette and the many in which it is smoked. Thus, it would not be unexpected to find the size distribution of smoke aerosols to vary considerably and be different from the ones generated in this study. Significantly greater attachment rates than those measured in this study might be encountered, especially if the smoke aerosol having larger size distribution are present.

Appendix A.

Measured physical parameters for the graded-screen battery are given in the table below.

Screen Mesh	Wire Diam (cm)	Thickness (cm)	Solid Fraction
LLL 6-screen:			
16	.04	.0978	0.199
50	.02	.0521	0.298
80	.0135	.0286	0.334
200	.0045	.0109	0.282
325	.003	.0086	0.331
500	.0026	.0048	0.421

Using these parameters the penetration of each stage as a function of particle size have been calculated according to Cheng(36). These values of penetration are used to establish the stage-penetration matrix for inversion of the diffusion battery data.

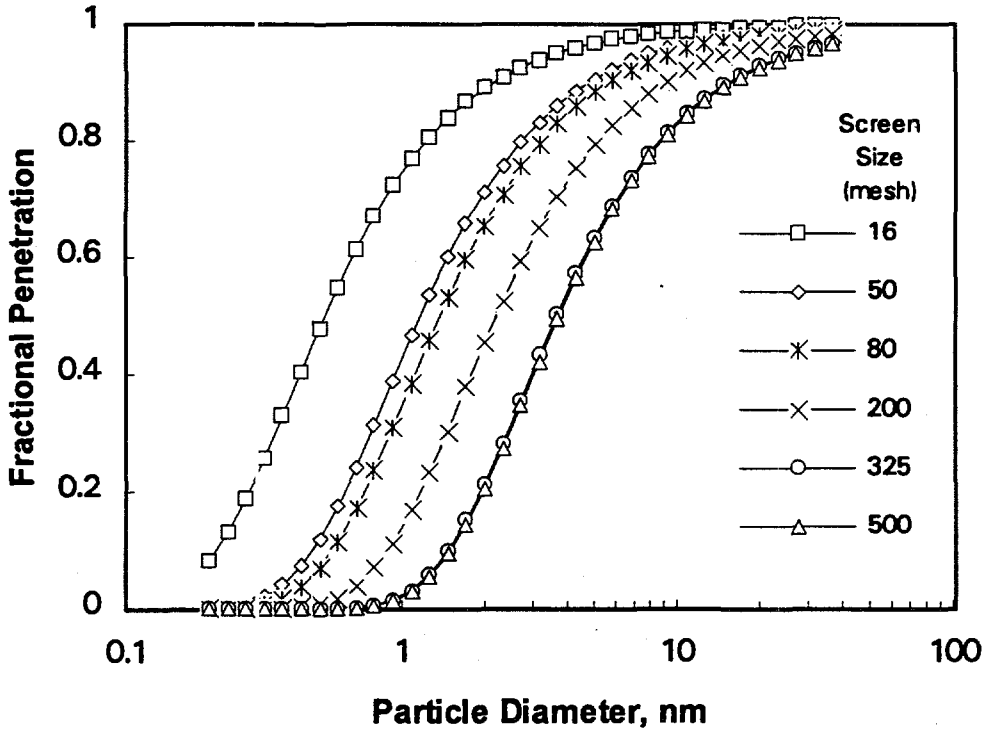

Acknowledgments

We gratefully acknowledge the support of our sponsor, the University of California Tobacco-Related Disease Research Program.

References.

1. Ueno Y. and Peters L.K. "Size and Generation Rate of Sidestream Cigarette Smoke Particles," Aerosol Sci. Tech., 5, pp. 469-476 (1986).

2. Hoegg U.R, "Cigarette Smoke in closed Spaces," Environ. Health Perspect., 1, pp. 117-128 (1972).

3. Hopke P. K., "Conceptual Design of a System to Characterize the Radioactive Ultrafine Aerosol," in Indoor Radon, Air Pollution Control Assoc., Pittsburg, PA, SP-54, pp. 206-215 (1986).

4. Porstendorfer J. and Mercer T.T., "Influence of Electric Charge and Humidity Upon the Diffusion Coefficient of Radon Decay products," Health Phys. 37, pp. 191-199 (1979).

5. Wellisch E. M., "The Distribution of the Active Deposit of Radium in an Electric Field," Philosophical Magazine 26, pp. 623-635 (1913).

6. Chamberlain A.C. and Dyson E.D., Br. J. Radio., 29, p. 317 (1956).

7. Raabe O.G., Nature, London 217, p. 1143 (1968).

8. Magee J.L. and Funabashi K., Radiat. Res., 10, p. 622 (1959).

9. Bloom J. and Margenau H., Phys. Rev.. 85, p. 670 (1952).

10. Mercer T.E. and Stowe W.A., "Radioactive Aerosols Produced by Radon in Room Air," in: Inhaled Particles III, p. 839 (1971).

11. Alshuler B., Nelson N., and Kusohner M., "Estimation of Lung Tissue Dose from the Inhalation of Radon and Daughters," Health Phys., 10, p. 1137 (1969).

12. Wagoner J.K., Archer V.E., and Carroll B.E., "Cancer Mortality Patterns Among US Uranium Miners and Millers, 1950 through 1962," J. Natl. Cancer Inst., 32, p. 787 (1964).

13. Katz R. and Hofmann W. "Thresholds in Radiobiology," Phys. Med. Biol., 27, p. 1187 (1982).

14. Saccomanno G., Huth G.C., Auerbach O., and Kuschner M.. "Relationship of Radioactive Radon Daughters and Cigarette Smoking in the Genesis of Lung Cancer in Uranium Miners," Cancer, 62, pp. 1402-1408 (1988).

15. Qiao Y., Taylor P.R., Yao S., Schatzkin A., Mao B., Lubin J., Rao J., McAdams M., Xuan X., and Li J. "Relation of Radon Exposure and Tobacco Use to Lung Cancer Among Tin Miners in Yunnan Province, China," Amer. J. of Indus. Medicine, 16 pp. 511-521 (1989).

16. Roscoe R.J., Steenland K., Halperin W.E., Beaumont J.J., and Waxweiler R.J. "Lung Cancer Mortality Among Nonsmoking Uranium Miners Exposed to Radon Daughters," JAMA, 262, pp. 629-633 (1989).

17. Selikoff I.J., Hammond E.C., and Chung J., "Asbestos Exposure, Smoking, and neoplasta," JAMA, 204, p. 106 (1968).

18. BEIR III, Committee on the Biological Effects of Ionizing Radiations, National Research Council, The Effects on populations of Exposure to Low Levels of Ionizing Radiation. National Academy Press, Washington, D.C. (1980).

19. ICRP, International Commission on Radiological Protection, Lung Cancer Risk from Indoor Exposures to Radon Daughters, ICRP-Publ 50, Pergamon Press, Oxford (1987).

20. Thomas D.C. and McNeill K.G., "Risk Estimates for the Health Effects of alpha-Radiation," Research Report INFO-0081, Atomic Energy Control Board, Ottawa (1985).

21. Whittemore A.S. and McMillan A., "Lung Cancer Mortality among U.S. Uranium Miners: a Reappraisal," J. Natl. Cancer Inst., 71, pp. 489-499 (1983).

22. Hornung R.W. and Meinhardt T.J., "Quantitative Risk Assessment of Lung Cancer in U.S. Uranium Miners," Health Phys., 52, pp. 417-430 (1987).

23. Sevc J., Kunz E., Tomasek I., Placek V., and Horacek J., "Cancer in Man after Exposure to Rn Daughters," Health Phys., 54, pp. 27-46 (1988).

24. Kopecky K.J., Nakashima E., Yamamoto T., and Kato H., "Lung Cancer, Radiation and Smoking among A-bomb Survivors of Hiroshima and Nagasaki," RERF Report TR 13.86, Hiroshima (1986).

25. Burkart, W., "Radiation Biology of the Lung," The Sci. of the Total Env.," 89, Chap 7, pp. 1-230 (1989).

26. Muller W.J., Hess, G.D., and Scherer P.W., "A Model of Cigarette Smoke Particle Deposition," Am. Ind. Hyg. Assoc. J., 52, pp. 245-256 (1990).

27. Biermann A.H., Thorngate J.H., and Sawyer S.R., "Participation in the 1989 Radon Daughter Workshop at the Environmental Measurements Laboratory," Lawrence Livermore National Laboratory, to be published in the HCD Annual Tech. Rev., UCRL-50007-90. (1991).

28. Nero, A.V., "Indoor Radiation exposures From Rn-222 and its Daughters: A View of the Issue," Health Phys., 45, p. 277 (1983).

29. Gesell, T.F., "Background Atmospheres Rn-222 Concentrations Outdoors and Indoors: A Review," Health Phys., 45, p. 289 (1983).

30. George, A.C. and Eng, J., "Indoor Radon Measurements in new Jersey, New York and Pennsylvania," Health Phys., 45, p. 397 (1983).

31. Nazaroff, W. and Nero, A., Radon and its Decay Products in Indoor Air, John-Wiley and Sons, New York (1988).

32. Jacobi W., "Activity and Potential Alpha-Energy of 222-Radon and 220-Radon-daughters in Different Air Atmospheres," Health Phys., 22, pp. 441-450 (1972).

33. Porstendorfer J., Wicke A., and Schraub A., "The Influence of Exhalation Ventilation and Deposition Processes upon the Concentration of Radon (222-Rn), Thoron (220-Rn) and their Decay Products in room Air," Health Phys., 34, pp. 465-473 (1978).

34. Holub R.F. and Knutson E.O., "Measuring Polonium-218 Diffusion-Coefficient Spectra Using Multiple Wire Screens," in Radon and Its Decay Products, ed. P.K. Hopke, ACS Symposium Series 331, American Chemical Society, Washington, DC, pp. 340-356 (1987).

35. Ramamurthi M. and Hopke, P.K., "On Improving the Validity of Wire Screen "Unattached" Fraction Rn Daughter Measurements," submitted to Health Phys. (1988).

36. Cheng Y.S. and Yeh H.C., "Theory of a Screen-type Diffusion Battery," J. Aerosol Sci.," 11, pp. 313-320 (1980).

37. Maher, E.F., "EM Algorithm Reconstruction of Particle Size Distributions from diffusion Battery Data," J. Aerosol Sci., 16, pp. 557-570 (1985).

38. Thorngate J.H., Radon Project: Detectors and Electronics, Lawrence Livermore National Laboratory, UCID-21782 (1989).

39. Thorngate J.H. and Biermann A.H., "Radon Project--Computer Programs for Acquiring and Reducing Data," Lawrence Livermore National Laboratory, UCID-21783 (1990).

40. Biermann A.H. and Sawyer S.R., "Measurement of Radon Progeny Size Distributions Using diffusion Batteries," Lawrence Livermore National Laboratory, to be published in the HCD Annual Tech. Rev., UCRL-50007-90. (1991)

41. Fuchs N.A., The Mechanics of Aerosols, The MacMillan Company, New York (1964).

42. Chen B.T., Namenyi J., Yeh H.C., and Mauderly J.L., "Physical characterization of Cigarette Smoke Aerosol Generated from a Walton Smoke Machine," presented at AAAR Annual Mtg., Chapel Hill, North Carolina, October 10-14 (1988).

43. George A.C., Knutson E.O., and Tu K.W., "Radon Daughter Plateout - I, Measurements," Health Phys., 45, p. 439 (1983).

44. George A.C., Knutson E.O., and Tu K.W., "Radon Daughter Plateout - II, Prediction Model," Health Phys., 45, p. 445 (1983).

45. Subba Ramu M.C., Muraleedharan T.S., and Vohra D.G., "A Study of the Attachment of Radon Daughter Atoms to Aerosol Particles," Pure Appl. Geophys., 122, pp. 133-140 (1984).

46. Raabe O.G., "The Adsorption of Radon Daughters to Some Polydisperse Submicron Polystyrene Aerosols," Health Phys., 14, pp. 397-416 (1968).

47. Raabe O.G., Concerning the Interactions that Occur Between Radon Decay Products and Aerosols, Health Phys., 17, 177 (1969).

48. Mercer T. T., The Effect of Particle size on the Escape of Recoiling RaB Atoms from Particulate Surfaces, Health Phys., 31, 173 (1976).

49. Junge C.E., Air Chemistry and Radioactivity, Academic Press, Inc., New York, NY (1963).

50. Biermann A.H. and Knutson E.O., Evaluation of Diffusion Coefficient Spectra Of ^{218}Po And ^{214}Pb Using Graded-Screen Diffusion Batteries, American Association of Aerosol Research 1991 Annual Meeting (1991).

51. Hidy G.M., Aerosols: An Industrial and Environmental Science, Academic Press, Inc., New York, NY (1984).

52. Morawska L. and Phillips C.R., Attachment of Radon Progeny to cigarette Smoke Aerosol, Aerosol Sci and Tech., 17, pp. 149-158 (1992).

53. Bruno R.C., Verifying a Model of Radon decay Product Behavior Indoors, Health Phys., 45, pp. 471-480 (1983).

54. Kojima H. and Abe S., Measurements of the Total and Unattached Radon Daughters in a House, Rad. Prot. Dos., 24, pp. 241-244 (1988).

55. Moller U. and Schumann G., J. geophys. Res. 75, 3013 (1970).

56. Chu, K. and Hopke P.K., Neutralization Kinetics for Polonium-218, Environ. Sci. and Tech., 22, pp. 711-717 (1988).

57. Saffman, P., and Turner, J.S., On the Collision of Drops in Turbulent Clouds, J. Fluid Mechanics, 1, 16 (1956).

58. Pnueli, D., Gurfinger, C., and Fichman, M., A Turbulent-Brownian Model for Aerosol Coagulation, Aerosol Science and Technology, 14, 201 (1991)

59. Dunn-Rankin D., Sidestream Tobacco smoke Dispersion and Inhalability, in Tobacco-Related Disease Research Program Annual Report to the Sate of California Legislature (1993).

60. Chang P., Peters L.K., and Ueno Y., Particle Size Distribution of Mainstream Cigarette Smoke Undergoing Dilution, in Aerosols, ed. Liu, Pui, and Fissan, Elsevier Science Publishing Co., Inc., New York (1984).

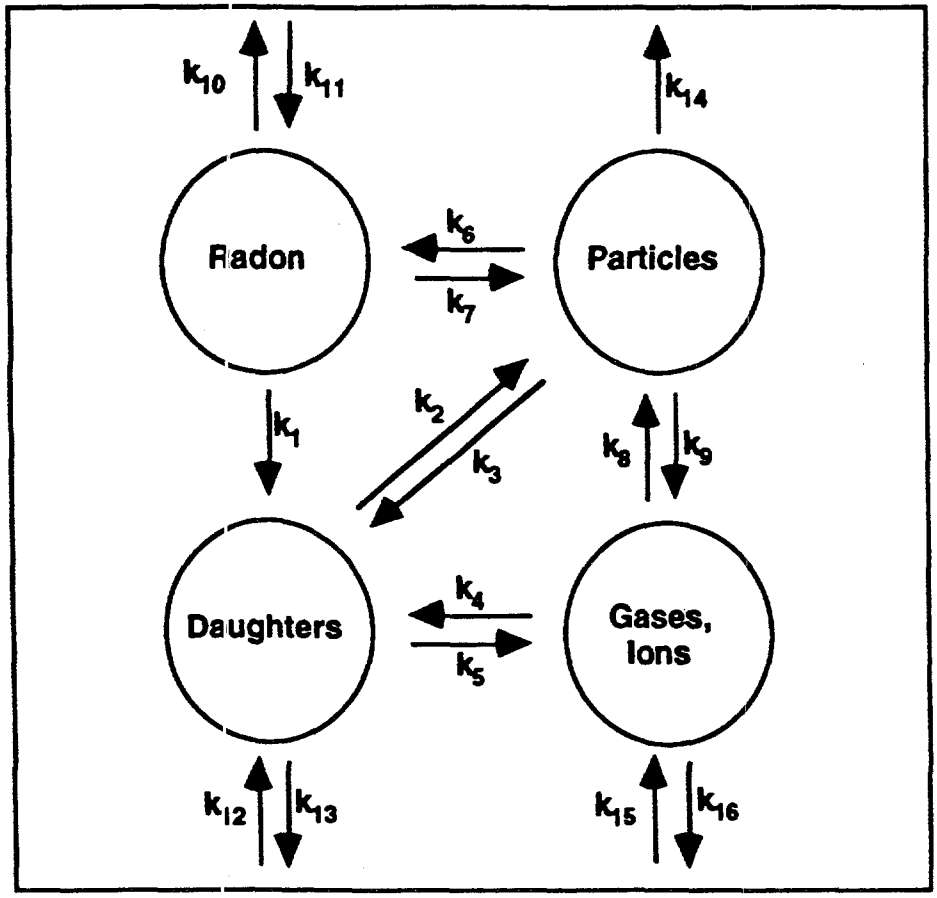

Figure 1. This schematic diagram illustrates the dynamic behavior of radon and its daugters in the environment.

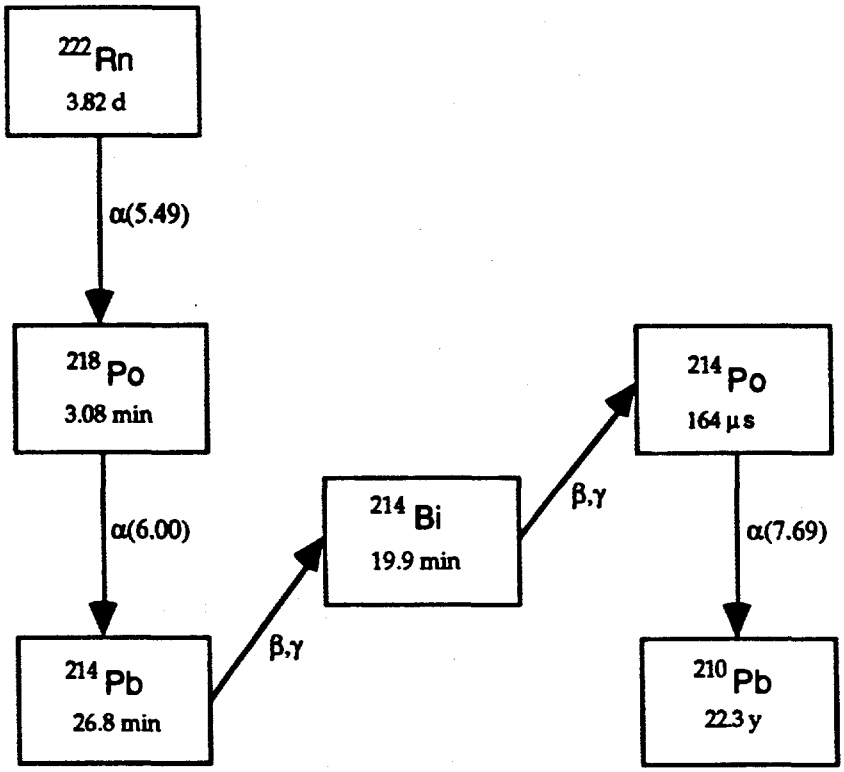

Figure 2. The radioactive decay scheme for radon and its daughters (through ^{210}Pb). Half lives and alpha decay energies (MeV) are indicated.

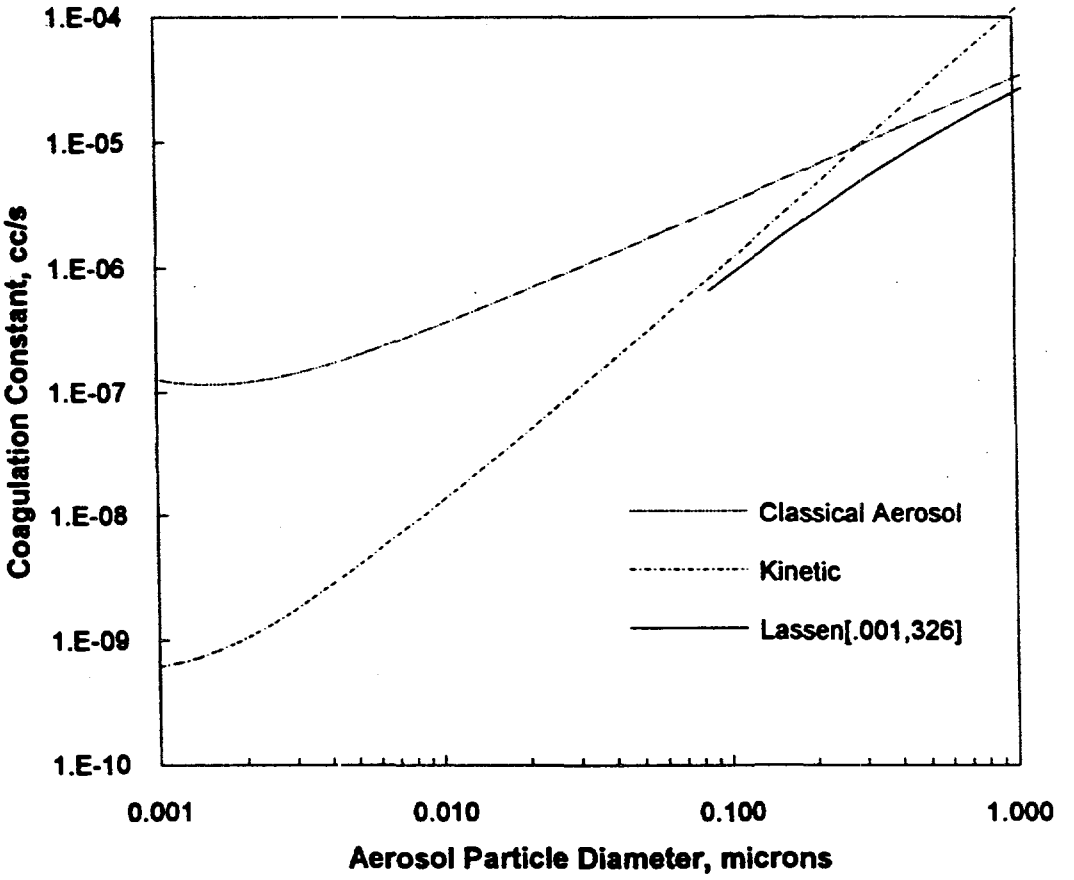

Figure 3. The Lassen and Rau attachment model bridges other coagulation theories in the submicron aerosol region.

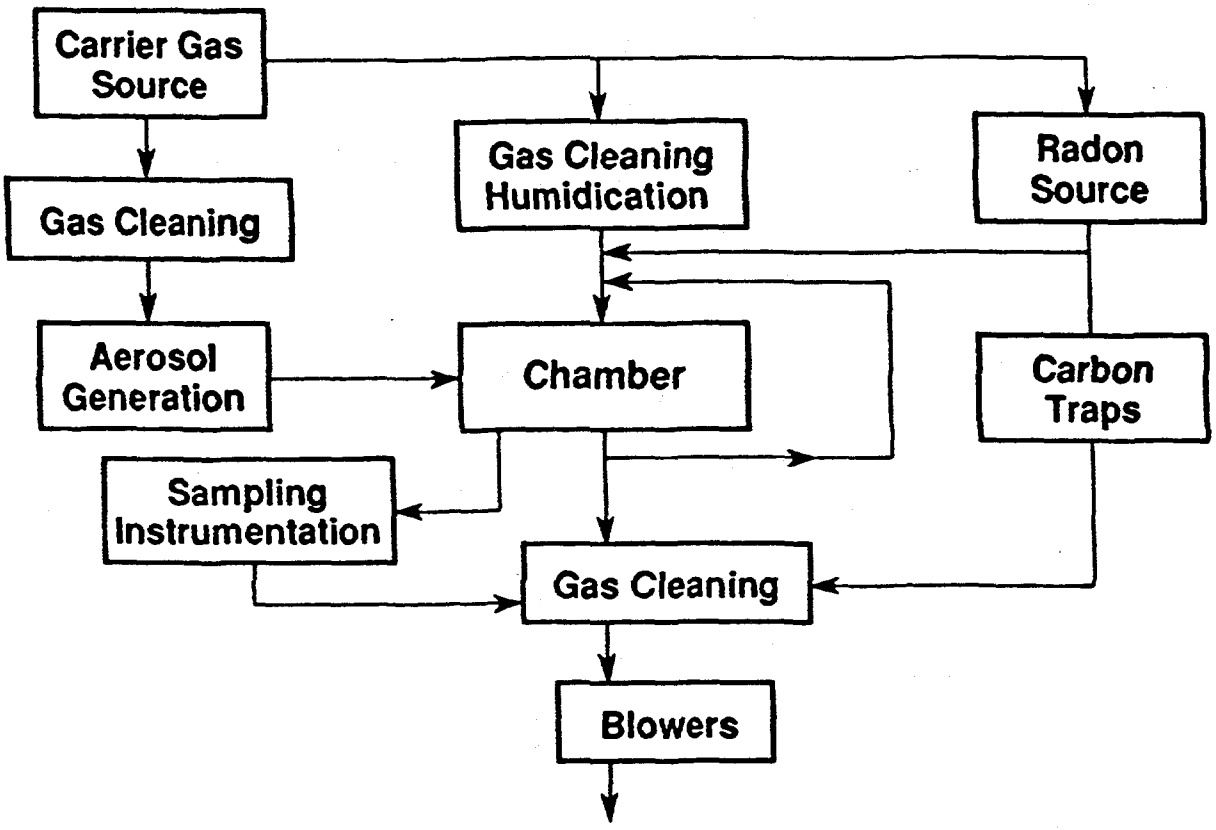

Figure 4a. Radon progeny attachment studies are performed using this experimental configuration.

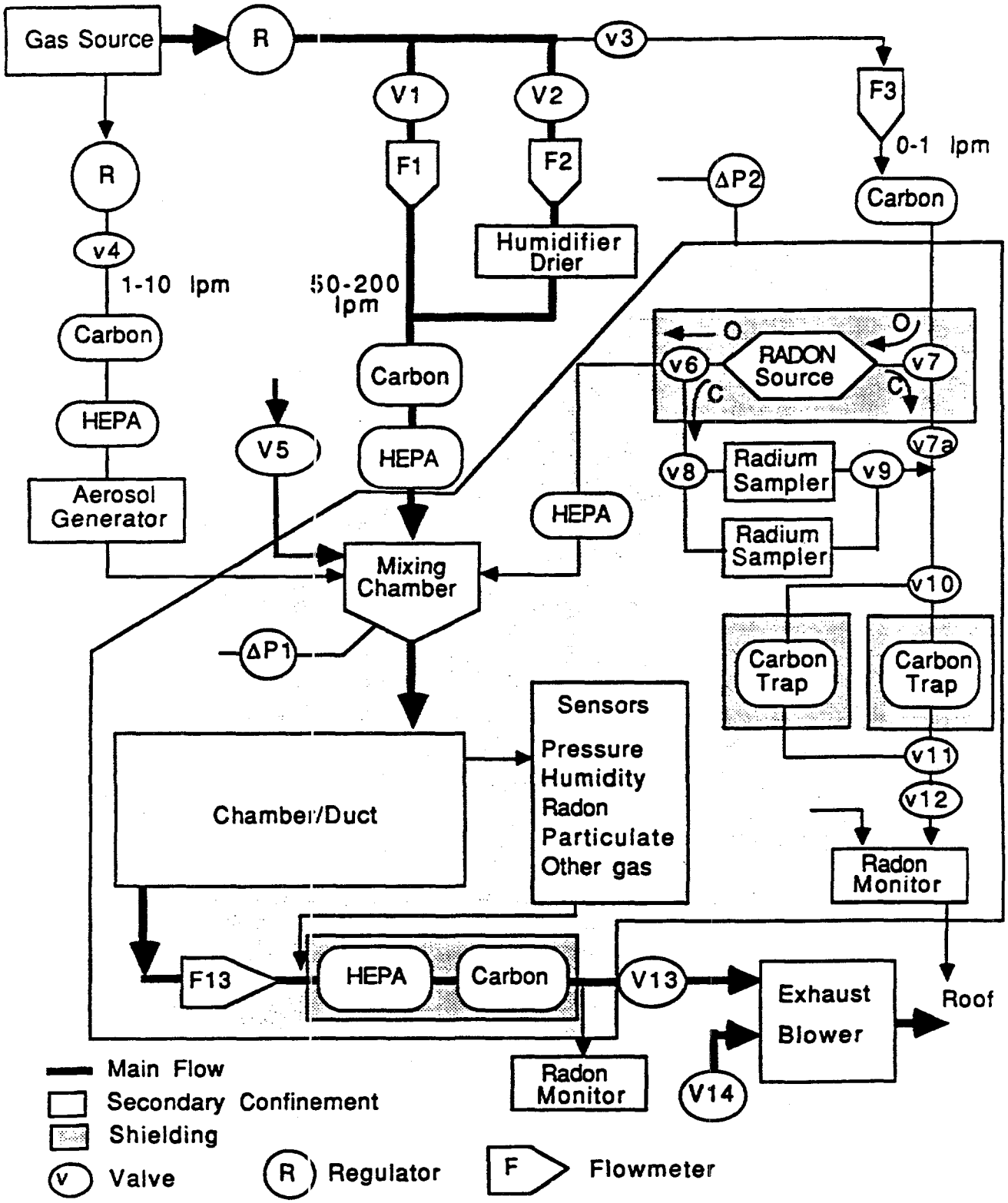

Figure 4b. Diagram of the Experimental Flow System.

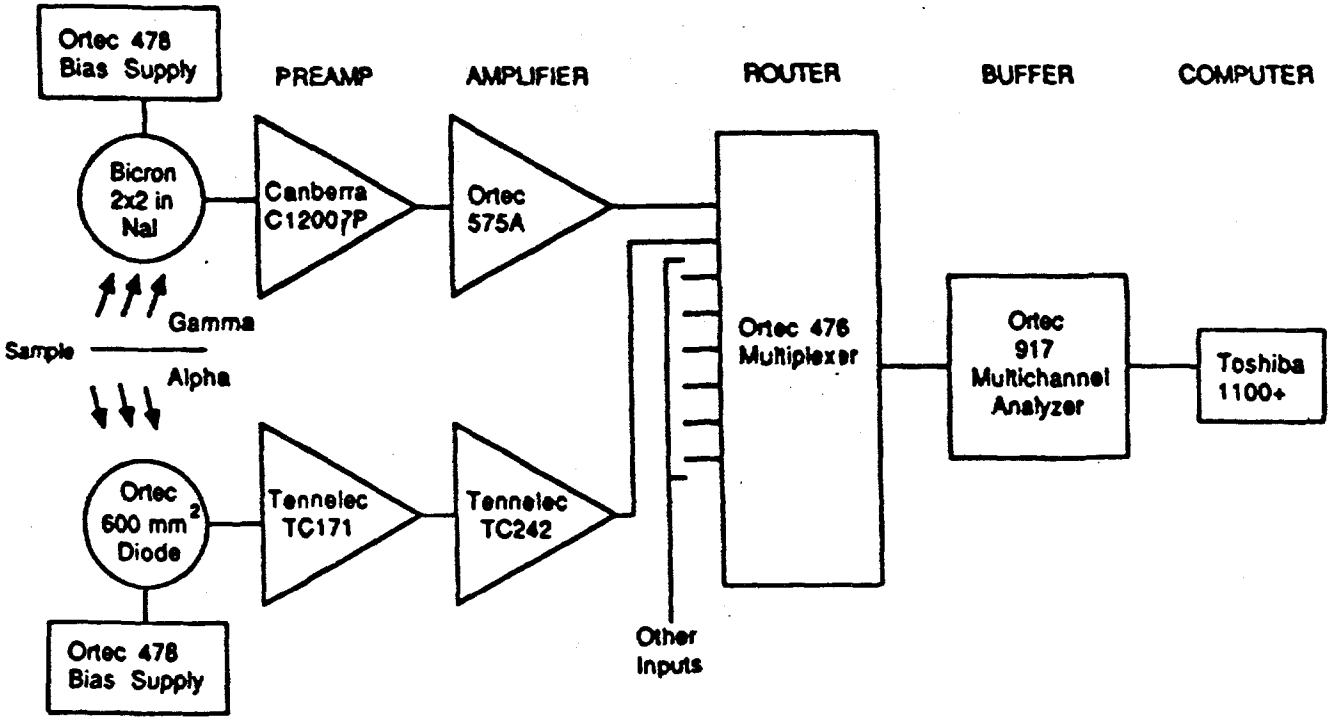

Figure 5. A block diagram of the alpha-gamma detector system.

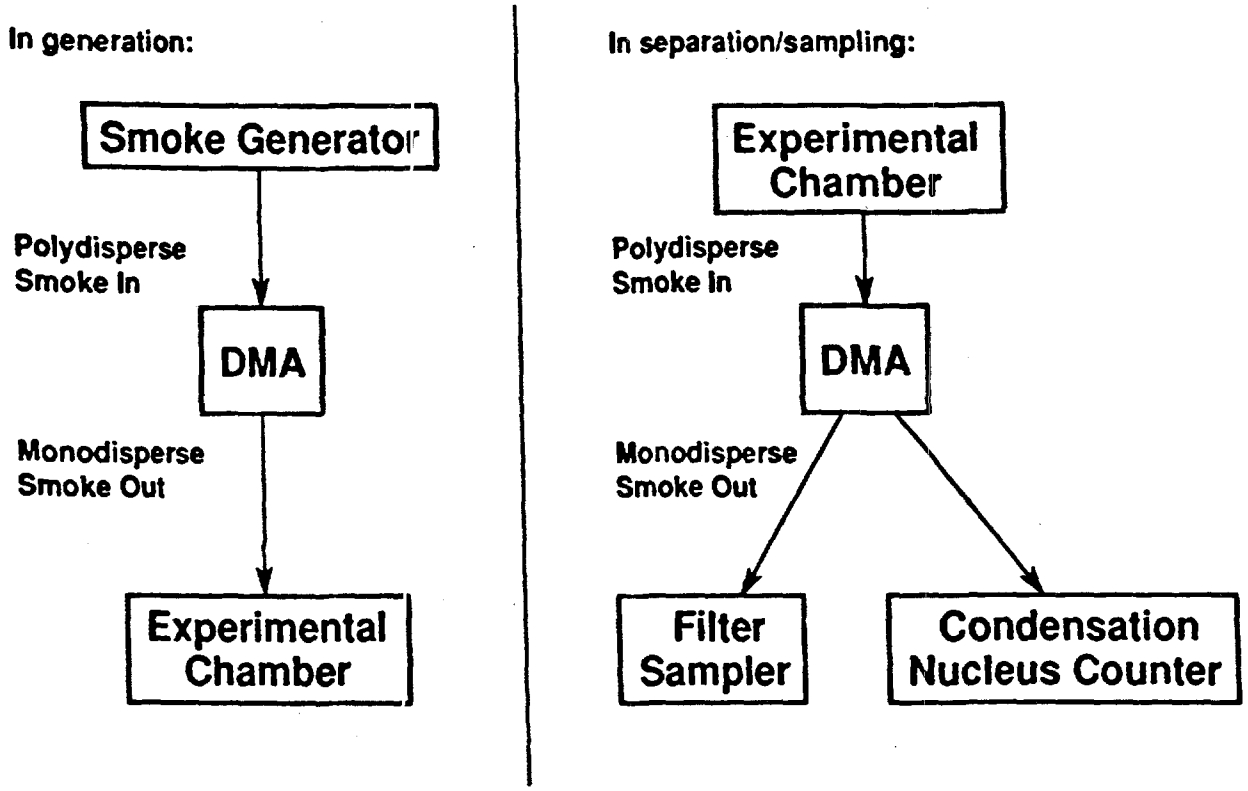

Figure 6. The differential mobility analyzer can be used for both aerosol generation and fractionation.

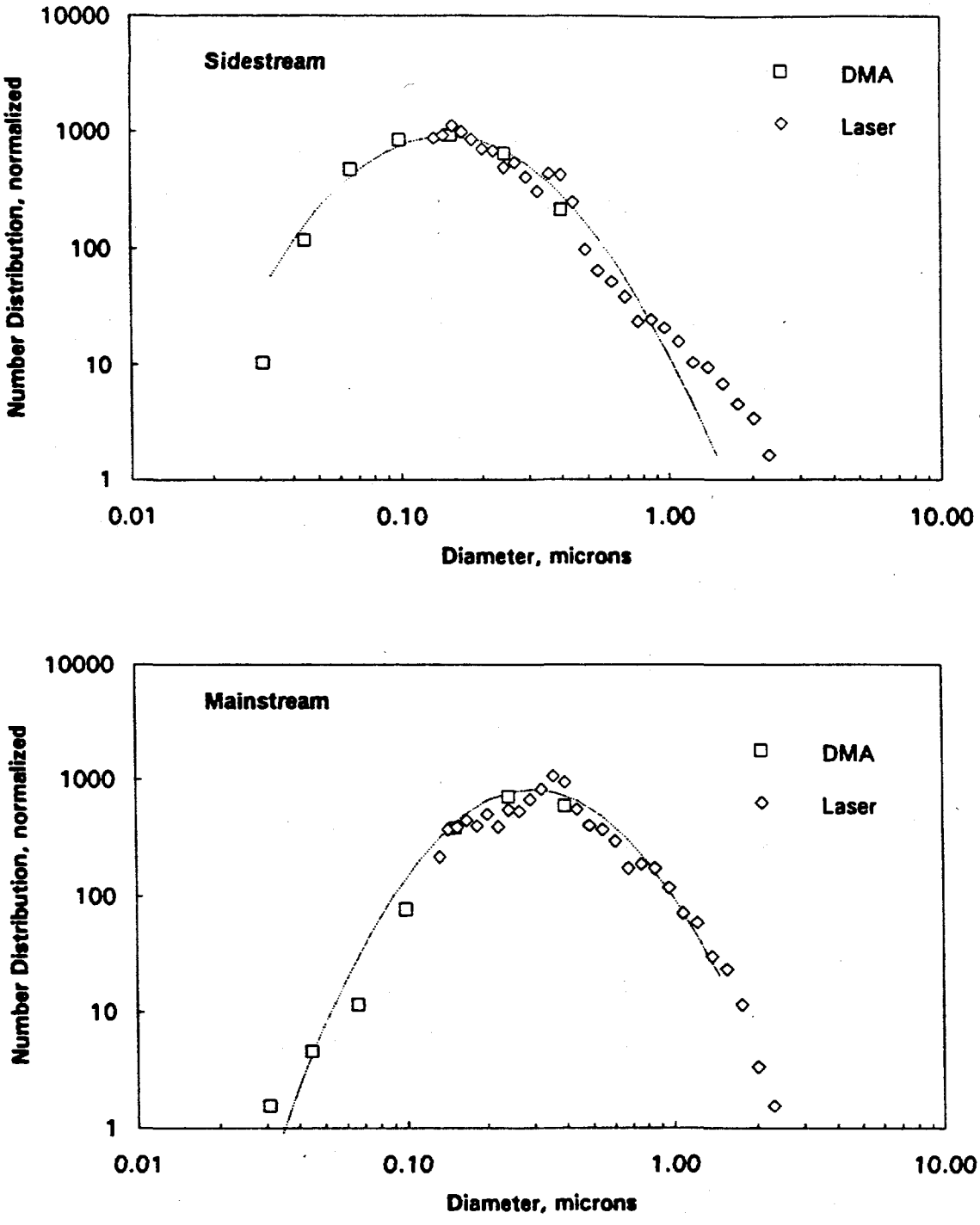

Figure 7. Comparison of the sidestream and mainstream cigarette smoke aerosol distributions. The data was obtained from both the laser spectrometer and the differential mobility analyzer.

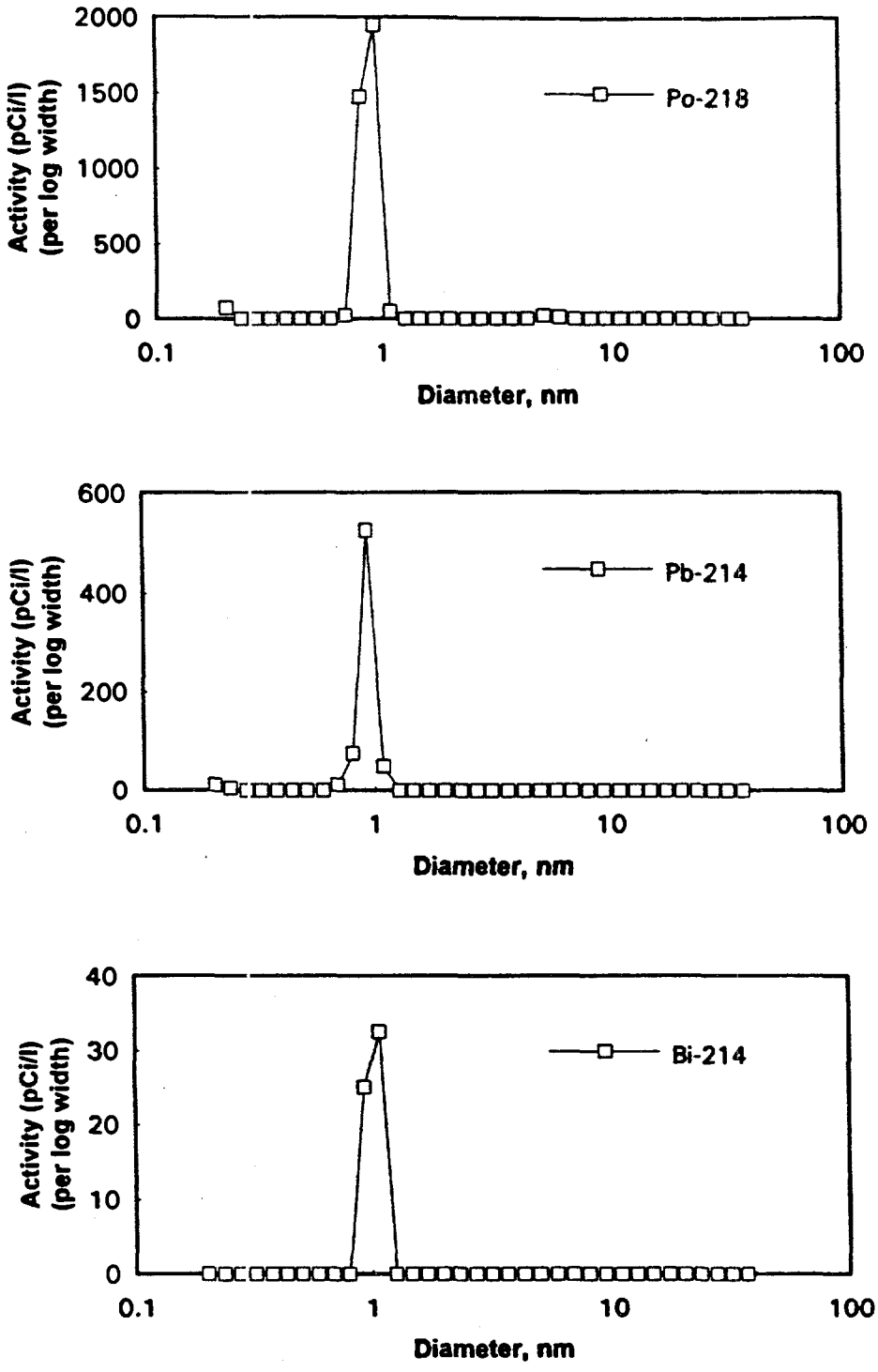

Figure 8. Size distriubtions of the radon progeny in a clean air environment are near monodisperse in the nanometer size range. data was obtained with the graded-screen diffusion battery.

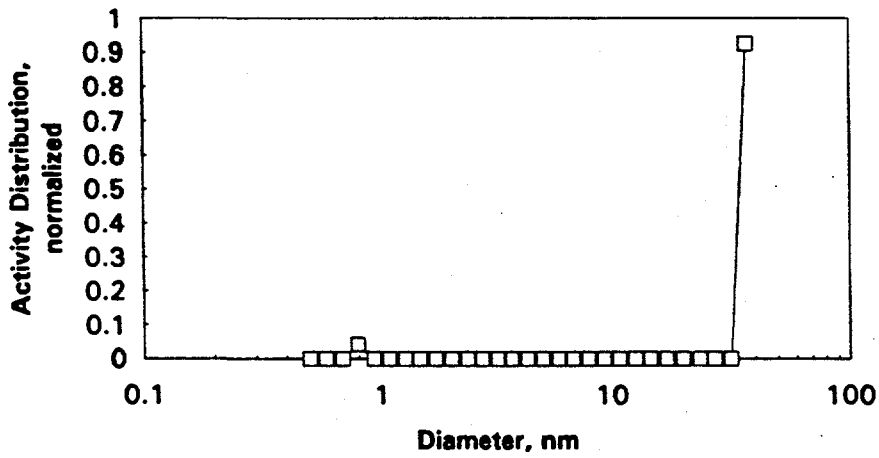

Figure 9. In the presence of a smoke aerosol, the graded-screen diffusion battery indicates a biomodal Po-218 activity distribution.

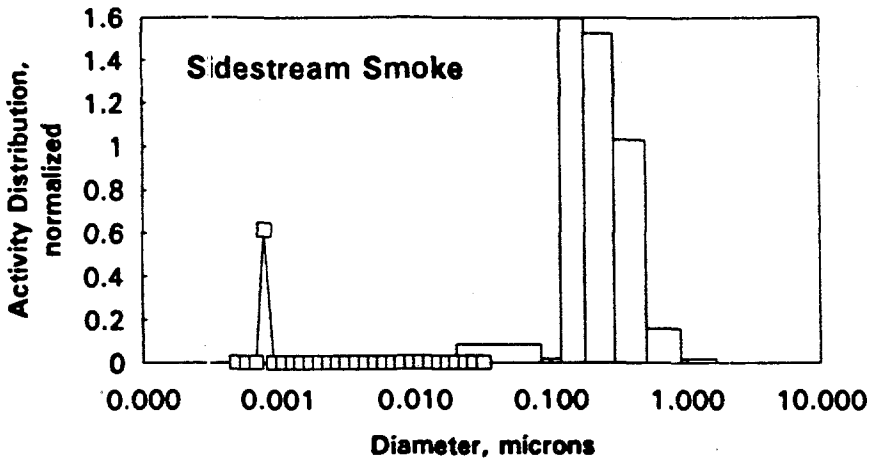

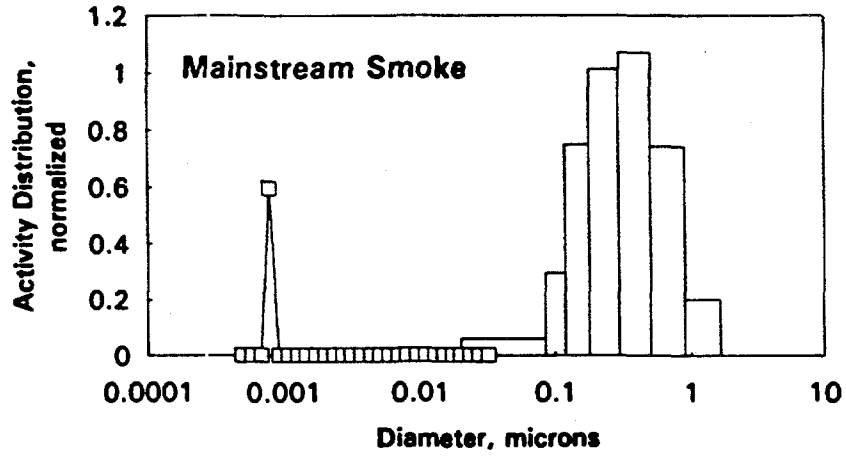

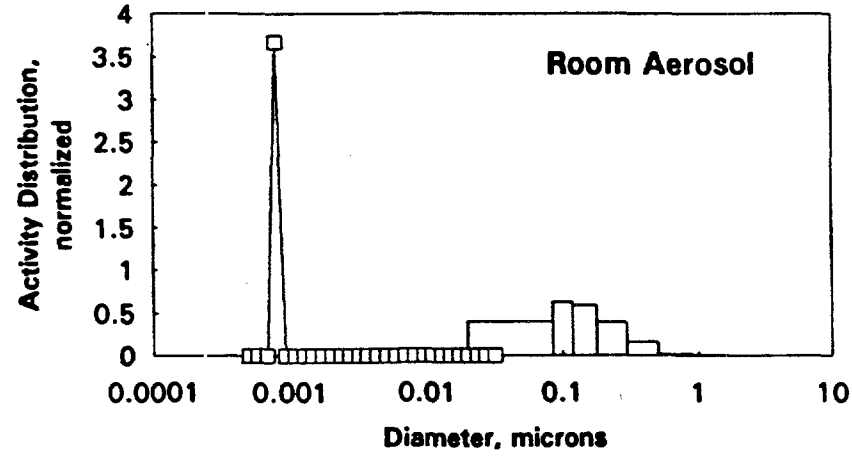

Figure 10. Composite activity distributions of data obtained from the diffusion battery and the rotating cascade impactor are compared.

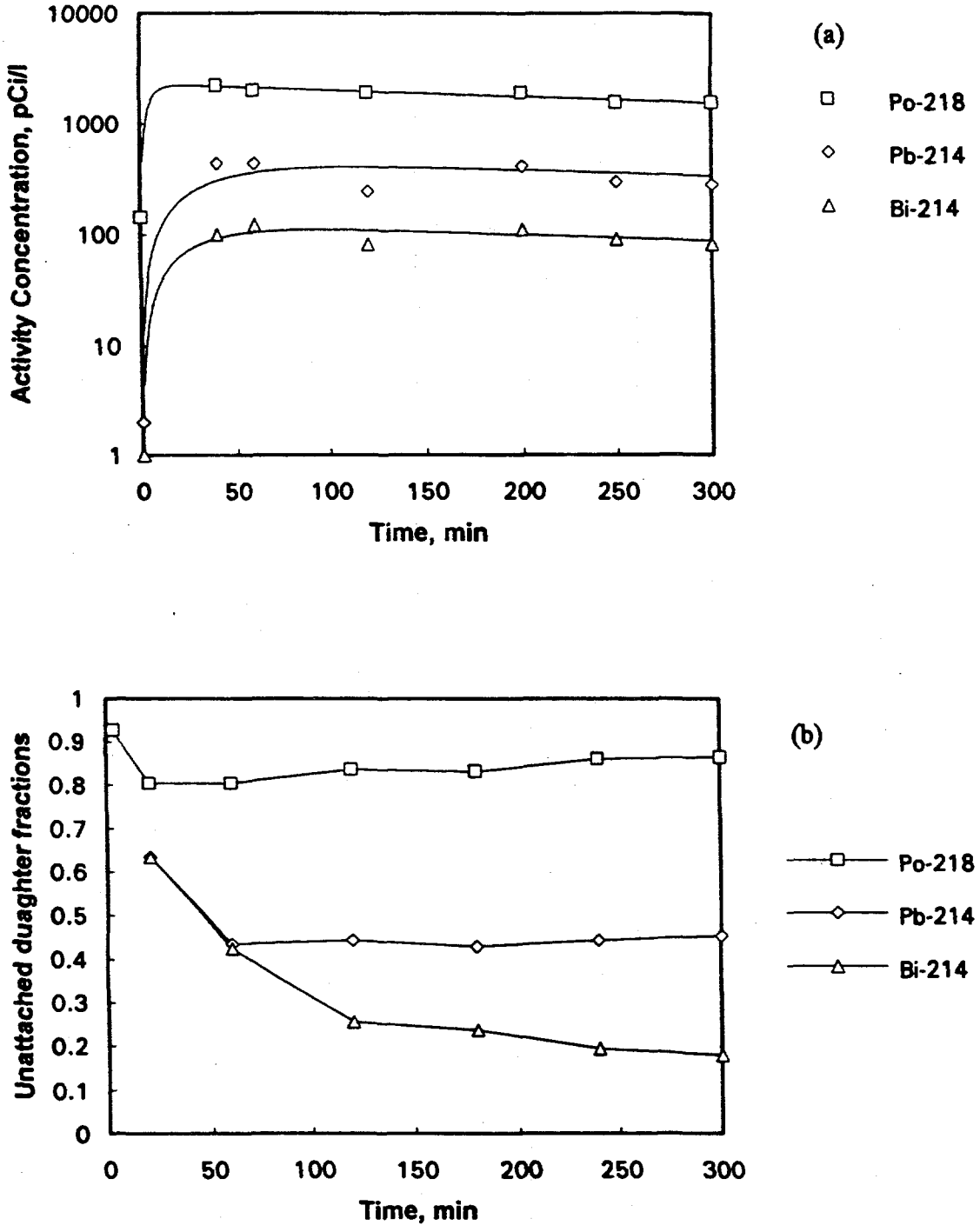

Figure 11. Interactions in the aerosol chamber approach steady-values.

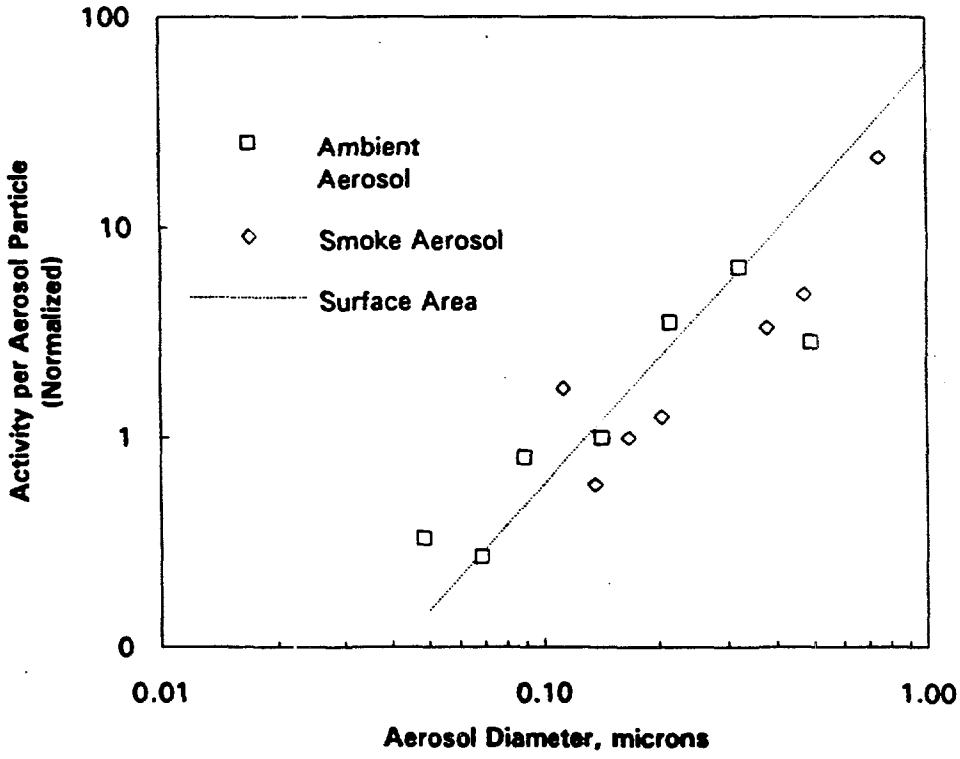

Figure 12. The behavior of radon attachment to differing particle sizes is illustrated for the cigarette smoke and the laboratory room aerosols.

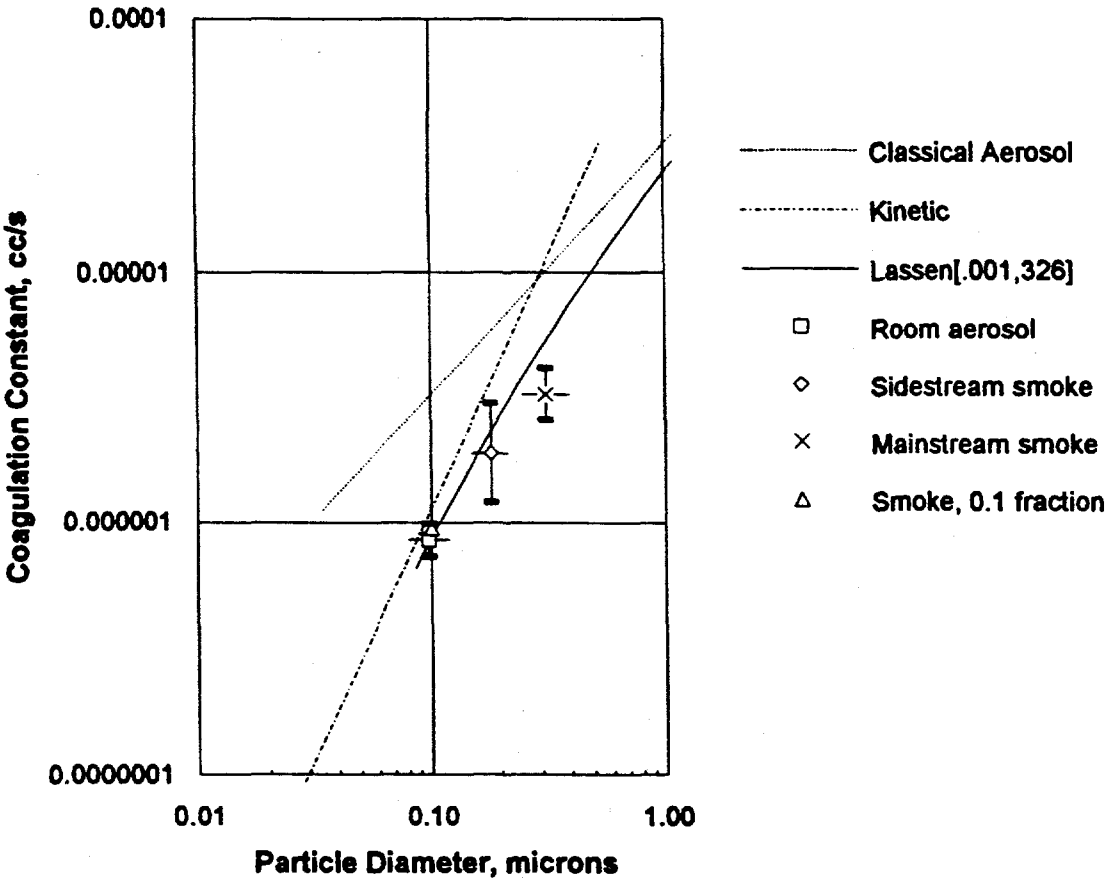

Figure 13. Values of absolute attachment coefficients compare favorably with theoretical expressions for aerosol coagulation.

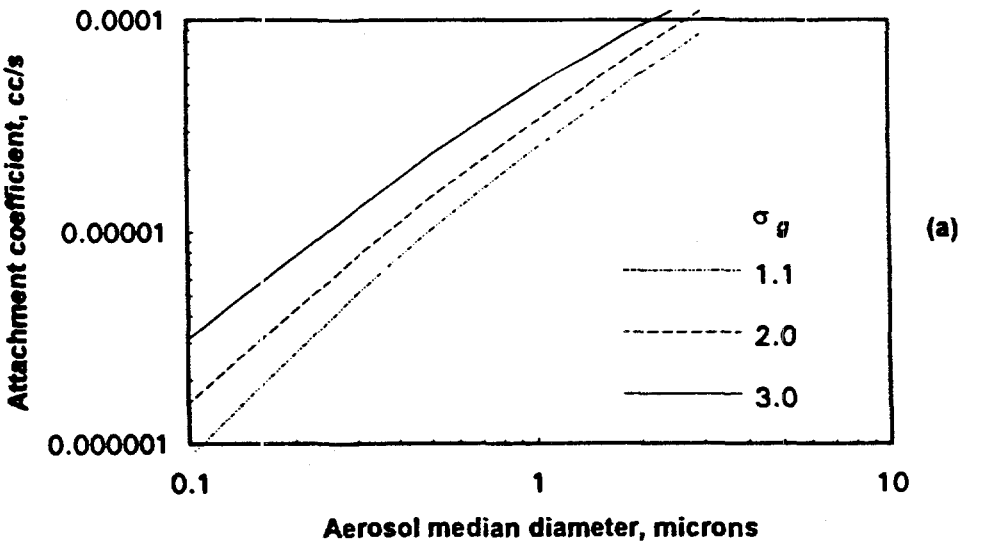

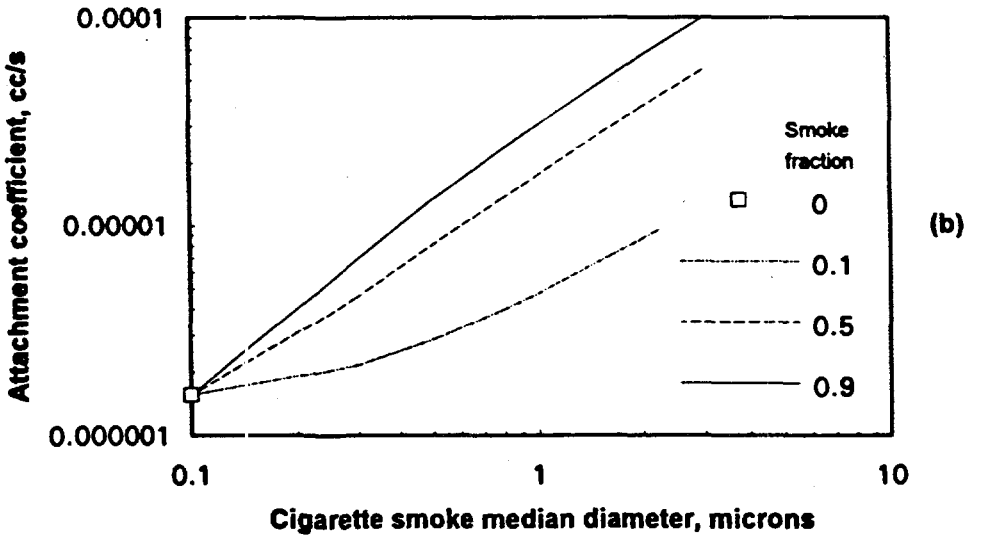

Figure 14. (a) The overall attachment rate of radon progeny to an aerosol increases with the median size and the standard deviation characterizing the aerosol distribution.
(b) In the presence of a fixed ambient aerosol, increases in the attachment coefficients also result with increased proportions of the cigarette smoke aerosol. The log normal parameters for the ambient aerosol were taken as $n_m = 0.1$ μm and $\sigma_g = 2.0$.